

A Preliminary Exploration Towards General Image Restoration

Xiangtao Kong^{3*} Jinjin Gu⁴ Yihao Liu¹ Wenlong Zhang^{1,3}

Xiangyu Chen^{1,2,5} Yu Qiao^{1,2} Chao Dong^{1,2 †}

¹Shanghai AI Laboratory ²Shenzhen Institutes of Advanced Technology, Chinese Academy of Sciences

³The Hong Kong Polytechnic University ⁴The University of Sydney ⁵University of Macau

{xiangtao.kong, wenlong.zhang}@connect.polyu.hk, jinjin.gu@sydney.edu.au,

{liuyihao, qiaoyu}@pjlab.org.cn, chxy95@gmail.com, chao.dong@siat.ac.cn

Abstract

Despite the tremendous success of deep models in various individual image restoration tasks, there are at least two major technical challenges preventing these works from being applied to real-world usages: (1) the lack of generalization ability and (2) the complex and unknown degradations in real-world scenarios. Existing deep models, tailored for specific individual image restoration tasks, often fall short in effectively addressing these challenges. In this paper, we present a new problem called general image restoration (GIR) which aims to address these challenges within a unified model. GIR covers most individual image restoration tasks (e.g., image denoising, deblurring, deraining and super-resolution) and their combinations for general purposes. This paper proceeds to delineate the essential aspects of GIR, including problem definition and the overarching significance of generalization performance. Moreover, the establishment of new datasets and a thorough evaluation framework for GIR models is discussed. We conduct a comprehensive evaluation of existing approaches for tackling the GIR challenge, illuminating their strengths and pragmatic challenges. By analyzing these approaches, we not only underscore the effectiveness of GIR but also highlight the difficulties in its practical implementation. At last, we also try to understand and interpret these models' behaviors to inspire the future direction. Our work can open up new valuable research directions and contribute to the research of general vision.

1. Introduction

We present a research problem called General Image Restoration (GIR). The primary goal of GIR is to develop a unified and systematic approach to address a wide

range of image restoration challenges that may arise in real-world applications. The objective of GIR is to transform any degraded input image into a corresponding natural and clear output. This encompasses not only individual image restoration tasks such as image denoising, deblurring, and super-resolution, but also the combination of these tasks, as well as real-world image degradations that are currently difficult to model. Given the limited existing literature on GIR, we need to construct the entire framework from scratch, including defining the problem, establishing evaluation protocols, developing baseline models, and interpreting these models. Before proceeding with these steps, it is crucial to specify our motivation for proposing the GIR framework.

Let us begin with the recent progress in image restoration. Benefiting from the fast development of deep learning techniques, individual image restoration tasks [22, 14, 25, 24] have enjoyed tremendous success in well-defined settings and constraint environments. However, they are still faced with the generalization problem and struggle to be applied in real-world usages [106, 124, 49, 69, 39]. Specifically, real-world images frequently present complex and unpredictable degradations, overwhelming most existing restoration models. For example, a hazy image might also exhibit defocus blur and JPEG compression, rendering a task-specific dehazing model insufficient for such complex cases. Furthermore, even if the hazy image does not contain other degradations, its haze feature might deviate from the training data distribution, leading to suboptimal results. The challenge of generalization is the primary driving force behind our proposal of the GIR problem. There is a pressing need for a comprehensive model capable of addressing diverse real-world challenges without necessitating specific parameter adjustments.

From another aspect, we can observe a similar trend in high-level vision. While conventional high-level vision tasks (e.g., image classification and object detection) have approached their performance bottleneck, general vision models (GVMs) came into view and developed at an astonishing speed. For example, INTERN [93] could deal

*This paper was done while the author was affiliated with Shanghai AI Laboratory and Shenzhen Institutes of Advanced Technology, CAS.

†Corresponding author (e-mail: chao.dong@siat.ac.cn)

with tens of vision tasks and achieve state-of-the-art performance with a single general model. Visual models based on multimodal language models can also complete a variety of visual tasks and have considerable intelligence. It is well believed that GVM is a promising direction to solve the generalization problem. Nevertheless, existing GVM experience and techniques are not suitable for image restoration. First, while other models take high-dimensional image data as input and obtain low-dimensional labels, image restoration models have both the input and output in the form of images. The generation of images is the problem that GIR needs to consider. Secondly, GVM extracts semantic information hierarchically from clear images, whereas image restoration models not only need to capture abstract semantic information but also handle pixel-level information in degraded images. More importantly, GIR is NOT a naive extension of multi-task problem! It should deal with real unseen data and complex degradation combinations, as depicted in Figure 1. Recently, there are also some low-level vision models similar to the concept of GVM have been proposed [21, 66]. Instead of focusing on restoration, they focus more on processing images from one modality to another.

With the above background, we can describe the necessities of studying GIR. First and foremost, GIR is a touchstone of generalization ability. As deep models are prone to overfit the training data, it is impossible to solve the generalization problem with a single-task model. GIR covers not only individual image restoration tasks but also their combined tasks (*e.g.*, deraining + denoising). Thus, it naturally favours the model with better generalization. On the other hand, when combining various tasks, we hope ideal deep models to learn the natural image distribution instead of specific degradations, providing a feasible solution towards a real general model. This also meets GIR’s requirements for intelligence. Except for the research value, GIR also has great application demand. Note that real-world scenarios usually cannot be synthesized by mathematical models. Complex and unknown degradations can appear in various forms, such as underwater blur and old film corruption, which cannot be processed by dedicated deep models. Therefore, we expect a general model that is powerful enough to handle real complex cases. Furthermore, it is also desirable for casual users to have a general model in hand, which can process most images without model selection.

To this end, we propose the new problem GIR and start with the most fundamental definition. At the beginning, we will clarify the differences between general high-level vision models, multi-task and blind image restoration models. After a detailed comparison, we can figure out the uniqueness of GIR. Then we will build the evaluation protocol, including degradation models, test datasets and evaluation metrics. This part mainly tells us “what tasks should be covered”, “where to evaluate the image quality” and “how to evaluate the generalization performance”. With such an

evaluation platform, we can benchmark existing potential methods. After careful investigation, we show the significance of GIR but find that most deep learning architectures and training strategies are not feasible for the GIR problem. It is also surprising that Transformers do not always outperform CNNs under such a complex setting. We also provide insightful discoveries from image restoration interpretation methods, such as LAM [36] and DDR [68]. These facts inspire us that we need completely different networks and training strategies to realize GIR, as well as to solve the generalization problem. We hope our work can lay the foundation towards a real general model in image restoration.

Our contributions can be summarized as follows:

1. We present a new GIR problem, which aims at processing unnatural and degraded images into natural and clean ones with one model. We discuss the necessity of GIR for real-world applications, and the uniqueness of GIR from existing technologies.
2. We provide a preliminary research framework for the GIR problem, including a simplified definition, dataset construction and evaluation methods. Our research framework allows us using existing techniques to explore GIR problems.
3. We build a benchmark for the existing possible GIR approaches. We verify the necessity, effectiveness and interpret the difficulties of GIR. Our results shed light on the future research of general vision.

2. Related Work

Generalization Problem in Image Restoration. Researchers have achieved great success in various individual image restoration tasks with mutually matched training and test sets, such as image denoising, super-resolution, deblurring, deraining, *etc.* [31, 51, 58, 77, 131, 125, 96, 126, 50, 30, 72, 81, 7, 113, 53, 87, 33, 65, 32, 94, 114, 121, 70, 17, 15, 118]. However, when the test degradation does not match the training degradation, many image restoration models will fail, *e.g.*, different downsampling kernels in super-resolution [37, 60, 49, 128], different noise distributions [1, 12] and different rain streaks [114, 39]. This lack of generalization ability poses a serious obstacle to the application of image restoration models, because the degradation of real-world input images is often different from the training set. Existing works either develop blind models to include more degradation possibilities during training, or bring the training data closer to practical applications. Existing blind restoration models often assume a pre-defined degradation model and assume that some of its parameters are unknown. However, the coverage of these degradation models is also very limited. For example, many blind super-resolution works assume that the blur kernel is Gaussian

[37, 60]. For situations beyond this range, these methods still face generalization problems. Another approach is to collect training images as similar to the real situation as possible [1, 8]. But this approach can only cover a very limited range of applications and is costly. Collecting training images for a broad range of applications is impractical. Only a little work has been proposed to study the reasons for the lack of generalization ability in image restoration. Kong *et al.* [49] propose to improve the generalization performance of SR networks by dropout layers. Liu *et al.* [68] present that networks tend to overfit to degradations and show deep degradation “semantics” inside the network. The existence of these deep degradation representations often means a decline in generalization ability. The utilization of this knowledge can guide us to analyze and evaluate the generalization performance [69]. Gu *et al.* [39] and Chen *et al.* [12] try different training strategies to understand the generalization of the derain and denoise task. Besides that, few works have been proposed to improve the generalization ability of models. Regarding cross-task generalization (specifically, handling degradation types not seen during training) there is no existing work.

Multi-Task Image Restoration. Multi-task image processing methods have been extensively studied. Three classes of work are closely related to the discussion in this paper. First, multi-task pre-training-based methods represented by IPT [13], EDT [54] and DegAE [67] are closely related to GIR. These methods utilize a shared backbone network for different tasks and replace different processing heads and tails for each task. Secondly, some methods [18, 123, 64, 76, 82, 55, 48, 20, 21, 66] use a unified structure to handle multiple tasks. Although they can handle multiple image processing tasks with one model, they only focus on specific tasks, and need to know degradation types. Thus, these methods cannot solve the generalization problem, nor can they handle cross-task or mixed situations. Another class of methods utilizes a network to learn tasks with complex degradations, such as Real-ESRGAN [106] and BSRGAN [124]. These methods consider the limited crossover between tasks and enable the network to generalise on these tasks. But for the cross-degradation of multiple broader tasks (*e.g.* noise + rain), we have yet to witness related work. Besides that, their evaluation systems are not clear and inadequate enough.

General Models and General High-level Vision. The development trend of artificial intelligence models is undergoing a paradigm shift from dedicated task-specific to general. First, general language models (GLM) have achieved impressive progress. Through large-scale pre-training, many models such as BERT [46] and GPT-3 [6], have demonstrated the potential of general models. These models greatly benefit a wide range of language-

related downstream tasks through task-specific fine-tuning and adaptation. Furthermore, with the task-independent training objectives and pretext tasks [42], the performance gain of pre-training can be increased by employing large-scale unlabeled data and a very large model. The success of GLM has also inspired the General Vision Model (GVM). GVM attempts to learn general representations in the computer vision field and use one general model to cover a wide range of vision tasks. Many previous works employ large-scale supervised [119, 90, 26, 95, 28], self-supervised [19, 35, 16, 23, 4, 11], and cross-modal [45, 83] pre-training and show generality on a limited scope of downstream vision tasks. Among these works, ViT-G [120] uses categorical supervision, SEER [34] applies contrastive learning between different augmented views, while CLIP [84] uses paired language descriptions, and INTERN [93] first learns expert models on different tasks and then integrates them into a general model. The main text discusses the difference between general image restoration and general high-level vision. These differences make it difficult to directly apply the experience accumulated in general high-level vision to the development of general image restoration. This paper has illustrated this from the perspective of definition, task construction and model analysis.

3. General Image Restoration

3.1. Definition

As general image restoration (GIR) is a new topic, we need to give it a primary and reasonable definition. Broadly speaking, we expect GIR to cover all image restoration tasks. However, many existing individual tasks even have different goals. For example, deraining task only focuses on the effect of rain removal. Hence even almost no-rain images of deraining test sets are suffered from compression artifact [114, 121], it is acceptable. But it is inapposite for GIR. (We discuss this state in Section 4.1 and Figure 2) GIR is not a simple mix of existing tasks. It needs to consider mixed degradation and focus on the common goal of restoration. Therefore, we first assume a desired image space (*e.g.*, natural and clear). The images in this space will be considered in line with human subjective aesthetic judgments. A GIR model can recover “commonly observed” degraded images to the corresponding desired natural and clean states, rather than focusing on a few specific types and ignoring the rest. To make this definition more concrete, we compare it to general high-level vision (GHV), multi-task image restoration (MIR), and blind image restoration (BIR).

GIR vs. GHV. Interestingly, the pipelines of GIR and GHV are somewhat symmetrical, as shown in Figure 1. Ideally, the output space of GIR and the input space of GHV are the same natural image space. By combining GIR and GHV, we can naturally work toward a general vision model. Moreover, the difference between GIR and GHV also lies

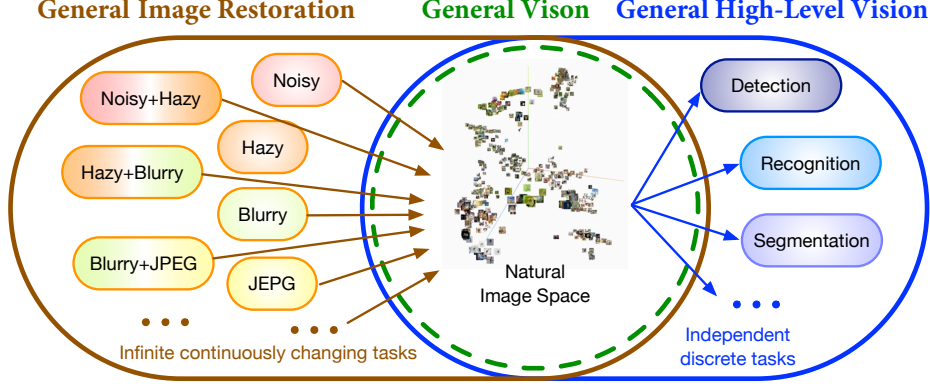


Figure 1: The differences between the General Image Restoration (GIR) and the General High-level Vision (GHV).

in their evaluation manner. GHV has clear human labels for accurate counting, but GIR needs to evaluate the image quality, which is subjective and ambiguous.

GIR vs. MIR. MIR is the closest concept to GIR in literature, but is different from GIR in two main aspects. First, they have different input image/task spaces. The input space for MIR is discrete (several pre-defined degradation/tasks), but for GIR it is continuous. MIR contains multiple disjoint restoration tasks, but GIR also includes their cross operations (e.g., denoise mixing deblur). Compared to the limited, well-defined tasks in MIR, the number of possible degradations in GIR is very large, as the combinations of degradations are nearly infinite. Second, the input information for MIR and GIR is also different. The model needs to know all the input degradation types beforehand for MIR. However, for GIR, the degradation information is unnecessary. The two differences above also apply to single-task restoration. In a word, GIR is a “blind” problem that covers a wide range of degradations and their combinations. It is impractical to assign task-specific parameters to different tasks.

GIR vs. BIR. As mentioned above, GIR is a “blind” problem. However, the most existing BIR methods are developed for a specific task, e.g., blind SR and blind deblurring. They usually adopt a known degradation model but treat the degradation parameters as to-be-predict factors. These methods also tend to take advantage of pre-defined degradation models as priors. But for GIR, we can not define such a parametric model. Most of the BIR methods (e.g., DAN [74, 75] and IKC [38]) cannot be directly applied to GIR. GIR should have an extensible pipeline to adopt any type of newly appeared degradations and have a clear evaluation system to evaluate generalization ability.

3.2. Problem objective

To better distinguish the objective of GIR from existing research objectives, we start with the objective of MIR problem. We represent the MIR input space as $\{\mathcal{X}^t\}_{t \in [T]}$, and the target image space as \mathcal{Y} where T is the number of tasks. The dataset is collected as $\{\mathbf{x}_i^1, \dots, \mathbf{x}_i^T, \mathbf{y}_i\}_{i \in [N]}$, where N is the number of data points, \mathbf{x}_i and \mathbf{y}_i are input and ground truth images. Similar to multi-task learning [92], the model is given for each task by $f^t(\mathbf{x}^t; \theta^{\text{sh}}, \theta^t) : \mathcal{X}^t \mapsto \mathcal{Y}$, where θ^{sh} is the model parameters shared between tasks and θ^t is the task-specific parameters. The loss function for each task is given by $\mathcal{L}^t(\cdot, \cdot) : \mathcal{Y} \times \mathcal{Y} \mapsto \mathbb{R}^+$. The current MIR paradigms generally yield the empirical risk minimization objective:

$$\min_{\theta^{\text{sh}}, \theta^1, \dots, \theta^T} \sum_{t=1}^T w^t \hat{\mathcal{L}}^t(\theta^{\text{sh}}, \theta^t), \quad (1)$$

where $\hat{\mathcal{L}}^t(\theta^{\text{sh}}, \theta^t) := \frac{1}{N} \sum_{i=1}^N \mathcal{L}^t(f^t(\mathbf{x}_i^t; \theta^{\text{sh}}, \theta^t), \mathbf{y}_i)$. This is an intuitive practice of MIR that can be implemented using a simple multi-objective weighted optimization method given the type of task. Accordingly, MIR evaluation only focuses on these tasks.

Compared to the MIR problem, the objective of GIR differs in two aspects. First, compared to the limited, well-defined tasks in MIR, the number of possible degradations in GIR is very large, as the possibilities of degradation combinations are nearly infinite. This implies that in GIR, the number of tasks $T^{\text{GIR}} \rightarrow \infty$. Second, due to the large number of potential tasks, it is impractical to assign task-specific parameters for each task. Thus the model parameters are shared among all tasks as θ^{GIR} . Let $\{\mathcal{X}^t\}_{t \in [T^{\text{GIR}}]}$ be the set of all possible tasks involved in the GIR problem. The objective formulation at this point can be written as

$$\min_{\theta^{\text{GIR}}} \sum_{t=1}^{T^{\text{GIR}}} w^t \hat{\mathcal{L}}^t(\theta^{\text{GIR}}) + \mathcal{G}, \quad (2)$$

where $\mathcal{G} := g(\hat{\mathcal{L}}^1(\theta^{\text{GIR}}), \dots, \hat{\mathcal{L}}^{T^{\text{GIR}}}(\theta^{\text{GIR}}))$ is a functional

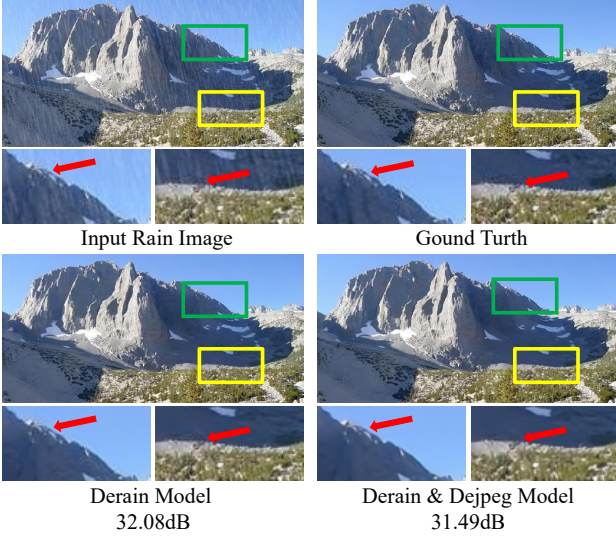


Figure 2: The Rain1200 result of models with different ability. The resulting image of derain&djpeg model obtains lower PSNR value, even though it looks more natural and cleaner. This issue arises from the reference GT images lacking the desired level of pristine quality and idealized perfection.

definition on the model space to measure the model’s generality. This generality term \mathcal{G} means that a GIR model should have acceptable performance on all covered tasks, rather than performing well on some tasks but failing on the others. However, in practice, we can only access a very limited number of tasks during optimization, *e.g.*, $T^+ \ll T^{\text{GIR}}$ accessible tasks. The GIR problem yields the objective of

$$\min_{\theta^{\text{GIR}}} \sum_{t=1}^{T^+} w^t \hat{\mathcal{L}}^t(\theta^{\text{GIR}}) + \mathcal{G} + \mathcal{R}, \quad (3)$$

where \mathcal{R} is the risk term of the model on tasks that cannot be sampled. \mathcal{R} is also a functional defined on the model space to represent the generalization ability of the model and may take many broad forms. Equation (3) exploits a similar idea of structural risk minimization to represent the objective of the GIR problem, that is, GIR should focus on the generalization ability and generality of the model.

Equation (3) not only provides a reference for us to develop GIR methods, but most importantly, it points out three important aspects of our GIR evaluation. First, we need to evaluate the effect of the GIR model in the tasks covered by the training set. It is the most basic aspect and is reflected in the first term. Second, we need to construct a suitable \mathcal{G} to evaluate the generality of the GIR model. Previous methods that simply compute the average across all tasks cannot objectively illustrate the generality of the model. Finally, we want to evaluate the performance of the GIR model outside the training set, which is what \mathcal{R} represents. There are many possible ways to integrate \mathcal{G} and \mathcal{R} into optimization.

In this work, we mainly discuss their form in evaluation. We hope to first establish a research framework to facilitate subsequent exploration.

4. Evaluation for General Image Restoration

In this section, we describe the evaluation protocol for the GIR approach. To evaluate the performance across tasks, we first contribute a test set containing selected tasks and testing images in Section 4.1. According to the problem objective in Section 3.2, we propose an effective approach to evaluate the generality \mathcal{G} in Section 4.2 and a feasible way for \mathcal{R} using the real-world data in Section 4.1.

4.1. Building GIR Test Set

Our test set contains both synthetic and real images. We use MiO100 [48] test set which contains 100 high-quality images including 10 scenes and select a series of different image degradations to construct 100 synthetic test sets (10,000 images in total). For the real images, we also collect 10 types of real-world testing images (each type contains 100 images, 1,000 in total).

Ground truth images. Many MIR works [52, 123, 64] directly use synthetic test sets (*e.g.*, Rain1200 [122] and RESIDE [53]) from each original single task. As mentioned in Section 3.1, we think these test sets are inappropriate for GIR and partial MIR tasks. Because the quality of the ground truth (GT) images can affect their evaluation. For example, as shown in Figure 2, the GT image from Rain1200 test set contains obvious JPEG compression artifacts. We can discover that the derain model removes rain but retains JPEG artifacts, while another derain&djpeg model can remove rain and JPEG artifacts at the same time. However, even though the derain&djpeg model obtained the result with better quality, it gets a lower PSNR value than the derain model result. This is because the results of the derain model are more similar to the GT, while the results of the derain&djpeg model are more different from GT. From this case, it can be seen that lots of so-called “GT” images in previous datasets are not actually “GT”. They suffer from various distortions, deviating from ideal natural and clean images. Note that, these test sets are acceptable for their original single tasks, since these single tasks only focus on their own degradations. However, they are inappropriate for MIR or GIR problems.

For GIR, the ground truth images should be the desired image state – high-quality natural images. Therefore, for synthetic images, we need high-quality images without any distortion and then synthesize low-quality images. Besides that, the GIR model is expected to perform well in a variety of different image content scenarios. However, the images in existing test sets often fail to cover a wide variety of scenes simultaneously. For these two reasons, we use MiO100 [48] test set which contains 100 high-

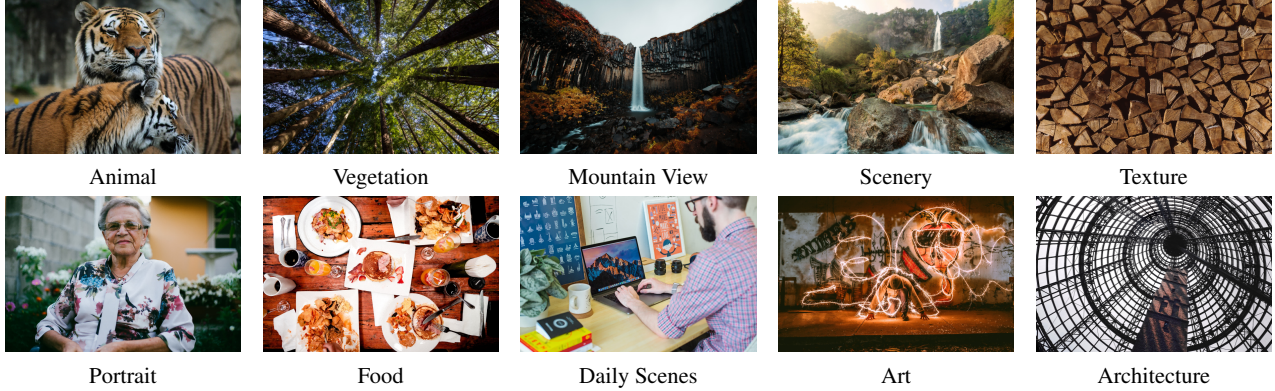


Figure 3: The demo of ground truth images. They contain 10 scenes with 10 images per scene from Unsplash [27].

quality images in a variety of different image content scenarios. These images contain 10 scenes with 10 images per scene from Unsplash [27]. As shown in Figure 3, these scenes encompass animal, vegetation, mountain view, scenery, texture, portrait, food, daily scenes, art and architecture.

Degradations. Recall that GIR aims to convert ‘commonly observed’ degraded images into their corresponding desired states, including degraded images from cross-operation between different degradations. We select a series of different image degradations to construct the test set. We hope that these tasks can: (1) cover most of the existing well-defined image restoration tasks; (2) focus on reasonable combinations and the mixture of them; (3) be representative for the feasibility of testing. Following these principles, we introduce the following designs.

1) *For the basic single tasks*, as shown in Table 2, we select 10 existing well-defined tasks according to their commonality. First, some of them are image degradations caused by digital image acquisition, sensor and storage limitations, *e.g.*, `resize`, `blur` and `noise`. These are the most common factors for image quality degradation and are almost inevitable. Second, we also consider the quality degradation of images under artificial post-processing, such as `compression`, `ringing` artifacts after image enhancement, and artifacts generated by restoration algorithms `alg.artifact`. Finally, we also include bad weather situations such as `rain`, `haze` and `snow`. This can help machine vision systems combat the degradation of the visual signal caused by external situations. A typical example is the vision system robustness of an autonomous driving system in bad weather.

These degradations are well modeled and there are many solutions available for reference, which is beneficial for building new tasks. On the other hand, the specific selection of ten tasks is not the key point, the point is that the degradations are already complex enough for helping existing methods to approach GIR. A GIR model should have

ID	Task Name	Scenario
(1)	<code>resize</code>	low-resolution.
(2)	<code>blur</code>	<i>e.g.</i> , motion blur, unfocus blur.
(3)	<code>noise</code>	<i>e.g.</i> , ISP noise.
(4)	<code>compression</code>	<i>e.g.</i> , JPEG artifacts.
(5)	<code>ringing</code>	ringing/over-sharpening artifacts.
(6)	<code>alg.artifact</code>	artifacts generated by restoration algorithms.
(7)	<code>damage</code>	parts of pixels are missing.
(8)	<code>rain</code>	visual information is obscured by rain.
(9)	<code>snow</code>	visual information is obscured by snow.
(10)	<code>haze</code>	visual information is obscured by haze.

Table 2: The list of the selected 10 basic single tasks.

the ability to solve these situations at least.

2) *For the combination and mixture tasks*, we propose a pipeline to synthesize various mixed degradation scenarios that may occur in the real world. Inspired by recent works [106, 124], we treat the degradation mixture as a composition of multiple basic degradation functions:

$$\mathbf{x} = (\mathcal{D}_k \circ \cdots \circ \mathcal{D}_2 \circ \mathcal{D}_1)(\mathbf{y}), \quad (4)$$

where \mathcal{D}_i represents the degradation function mentioned above with different hyper-parameters, k is the order number of degradation process. Eq. (4) is intuitive. The quality degradation of an image may be the result of multiple operations. For example, taking a photo on a hazy day, the image is enhanced by algorithm processing, resulting in the ringing artifacts, and then compressed during network transmission. Such a complicated process cannot be simply modeled with single pre-defined degradation models. In fact, images may go through a random number of random degradation processes. In our pipeline, we introduce this stochastic mechanism to cover the possible cases as much as possible. There is only one known exception. The degradations of `rain`, `haze` and `snow` cannot be added afterwards, but only appear in the process of image acquisition. Therefore, they can only appear as the first degradation process \mathcal{D}_1 .

3) *Select representative tasks for testing.* The combination of degradations makes it impractical for us to test on all tasks. In fact, due to resource constraints, we can only test on very limited representative tasks. Also, we cannot arbi-

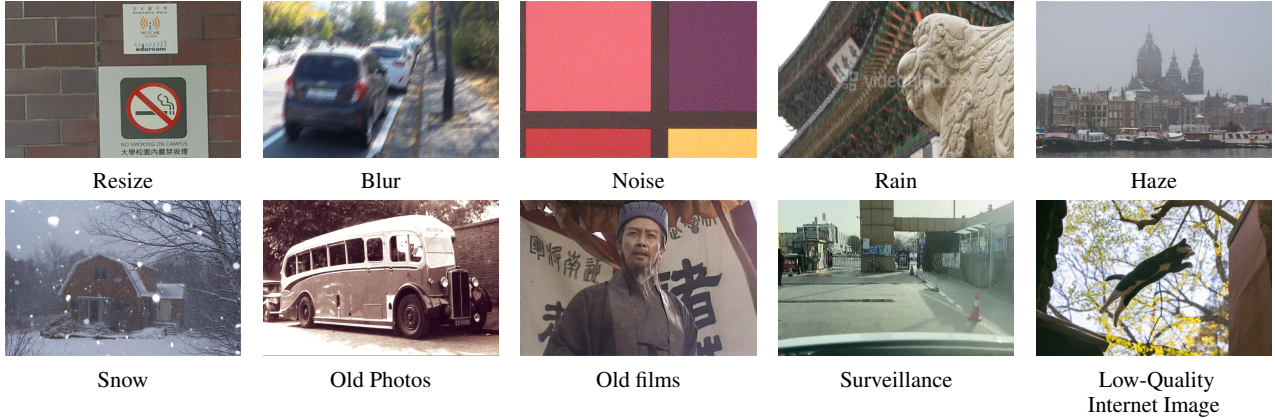


Figure 4: The demo of real world images. They contain 10 types with 100 real-world testing images per type.

trarily select a small number of tasks for testing, because a few samples are unable to represent the whole degraded image space and one may only select cases in their favour to compare, resulting in nonobjective and unfair comparison. We propose to select a subset of representative test tasks (or degradation types), which have large inter-task distances, to cover a wide range of degradation space. We first include the above 10 single tasks with selected parameters. Second, for mixture tasks, we sample a large number of possible mixture tasks following Eq. (4) with order k . We conduct spectral clustering analysis [79, 100] on these generated mixture tasks as different degradation combinations may lead to similar visual results. We select the clustering centers as the representative testing tasks. The detailed process is in the appendix.

The order k in our experiments samples from 2 to 5. For each k , ten representative tasks are collected. As a result, we select 50 representative tasks including the single tasks. In addition to 50 representative tasks, we collect the other 50 randomly generated degradations following Eq. (4) for each order from $k = 1$ to $k = 5$ for testing and cross-validation. The differences in model performance between the clustering center set and the cross-validation set can often indicate generalization issues. These 100 degradations/tasks cover a wide range of testing scenarios. The detailed degradation formulations, parameters and visual demos are shown in the appendix.

Real-world test images. Evaluating real-world scenarios is a feasible way to measure \mathcal{R} of Eq. (3) which represents the situations that can not be sampled. Therefore, we also collect 10 types of real-world testing images. For some of the single tasks involved, there has been a lot of works proposing real-world datasets for them. GIR should show better results on these datasets. As shown in Figure 7, we include the RealSR dataset [8] for task `resize`, the GoPro [78] and the RealBlur [89] dataset for task `blur`, and the SIDD [1] for `noise`. We can access the ground truth for reference in these test sets. We also include the SPA dataset [105] for `rain`, [53] for `haze` and [71] for

`snow`. For these data, we have no ground truth as the reference. We also collected additional degradation types that are not present in previous studies, *i.e.* old photos, old films, surveillance and low-quality Internet images. These images without corresponding ground truth mostly come from the Internet, with a small part from [111] and [101]. For the real-world testing images, we use the non-reference IQA methods such as NIQE as metrics to reflect the reconstruction performance.

4.2. Evaluating Model Generality

To evaluate the performance of MIR and BIR, previous works [57, 49] directly calculate the average performance on a randomly-sampled small-sized test set. However, we note that the average PSNR is not entirely sufficient for GIR because a higher average PSNR may be obtained by performing well on only a portion of the tasks, without maintaining model generality. We want to achieve a balanced and acceptable performance across various tasks that GIR can cover, instead of focusing on only a part of tasks and sacrificing performance on the other tasks. Thus, in Eq. (2), the generality term \mathcal{G} is added to the evaluation of GIR. Here we give a simple and reasonable choice of \mathcal{G} .

As different degradations may have different quantitative results (*e.g.*, PSNR), absolute numbers are no longer reliable indicators. The average quantitative results across all testing samples will lead to misleading comparison results for GIR evaluation. We need baselines and hope that they can describe the performance expectations of using a simple deep model on a task, and the performance we can expect to obtain when using a relatively good deep model. Similar to SEAL [129], we introduce an acceptance line and an excellence line to evaluate the overall performance of GIR. For every single task t , we train a three-layer convolutional deep network [31] supervised without any multi-task setting. Then we record its testing loss $\hat{\mathcal{L}}^t(\theta^{\text{AC}})$, defining this as the acceptance line. For the excellence line, we replace the shallow network with a more advanced deep residual network [43]. The performance of this network is recorded as the excellence line $\hat{\mathcal{L}}^t(\theta^{\text{EXC}})$. The generality is mea-

sured by comparing the GIR model with the acceptance line and excellence line and see on how many tasks GIR can meet our requirements for acceptance and excellence. These ratios are also called the acceptance ratio (AR) and the excellence ratio (ER) as

$$\text{AR} = \frac{1}{T^{\text{Test}}} \sum_{t=1}^{T^{\text{Test}}} \mathbb{1}\{\hat{\mathcal{L}}^t(\theta^{\text{GIR}}) \geq \hat{\mathcal{L}}^t(\theta^{\text{AC}})\}, \quad (5)$$

$$\text{ER} = \frac{1}{T^{\text{Test}}} \sum_{t=1}^{T^{\text{Test}}} \mathbb{1}\{\hat{\mathcal{L}}^t(\theta^{\text{GIR}}) \geq \hat{\mathcal{L}}^t(\theta^{\text{EXC}})\}, \quad (6)$$

where $\mathbb{1}\{\cdot\}$ is the indicator function. Specifically, for the 100 select testing tasks, we train 100 models for the acceptance line and 100 models for the excellent line. The generalizability and overall performance of the GIR model can be effectively measured by leveraging the relative referencing metrics of AR and ER across the degradation space.

Discussion. In this section, we propose an evaluation framework for GIR problem, including 110 test tasks (100 synthetic and 10 real tasks) and two new evaluation metrics AR and ER. In terms of data, this approach is more representative of model performance across the entire degradation space. Previous methods usually use the results of a few selected degradation to represent the performance [49, 124, 52]. In terms of metrics, previous methods often directly compare the PSNR values. However, our evaluation framework incorporates generalization into consideration. ER/AR not only allows a fair comparison between GIR models but also measures the overall progress of GIR development. When ER/AR is close to 1, we can tell that a GIR model could be comparable to simple/common single-task models. Of course, even both ER/AR has reached 1, it does not demonstrate that GIR is realized. But under the current conditions, increasing ER and AR should naturally encourage the models to improve their generalization ability and move toward GIR.

5. Benchmarking Existing Approaches

By formally defining the task of GIR and establishing a comprehensive evaluation protocol, we can conduct a comprehensive benchmarking of various existing methods that could potentially be adapted or leveraged for the GIR task. We first investigate the existing approaches and select the methods that meet the model principle in Section 3. Then we refine and retrain them based on the GIR dataset. Note that, the retraining process employs a straightforward strategy across all models, without incorporating any specialized techniques or tricks. Finally, we show the performance of these methods and analyze the experimental results. The purpose of the benchmark is not to propose a new method, but rather: (1) to verify the feasibility and importance of GIR; (2) to demonstrate the practical difficulties of GIR at the current stage and emphasize the importance of general-

ization; and (3) to identify potential future research directions by exploring existing approaches.

5.1. Implementation

Method investigation. Due to the novelty of GIR, we do not have an off-the-shelf method that can be directly applied. Fortunately, we have learned the basic principles of choosing a method according to the discussion in Section 3. Because the degradation information is not available for a GIR model, most methods that require auxiliary information input, such as, conditional restoration models [127, 40, 41] are ruled out. Similarly, methods that involve pre-training on a large dataset followed by fine-tuning on specific tasks [13, 54, 67], or a mixture of expert methods, also cannot meet our requirements. Because it is impractical to assign task-specific parameters to different tasks due to a large number of tasks. We can only assume a large model with shared parameters across tasks and aim to build a fully “blind” model.

As mentioned in Section 3, the most current blind restoration methods cannot be directly applied to GIR. However, we find some exceptions. DASR [104] does not assume an explicit degradation model and learns degradation information by contrastive learning which can theoretically cover any type of degradation. Recent works BSRGAN [124] and RealESRGAN [106] provide a simple and practical way to directly integrate a large number of tasks in the training of a powerful image-to-image network. We find that this approach can be directly extended to GIR. Finally, we select DASR [104] and several representative powerful backbones including RRDB [107], SwinIR [56], Restormer [117], Uformer [109] and HAT [22] to be benchmarked and the training method of BSRGAN [124] and RealESRGAN [106] is employed to retrain these backbones.

Training strategy. For the training strategy, we use a training strategy similar to BSRGAN [124] and RealESRGAN [106]. We synthesize the training image pairs according to the method described in Eq. (4). During training, we sample the clean ground truth images from DIV2K [3] and Flickr2K [97] datasets, including 3,450 2K images in total. We generate images with rain, haze and snow offline because these degradations need global information about the images to adjust parameters or estimate depth. The remaining degradations are applied to image patches on the fly with a wide range of random parameters. During training the models, l_1 -norm loss function [108] is adopted with the Adam optimizer [47] ($\beta_1 = 0.9$, $\beta_2 = 0.999$). The batch size is set to 8, and the patch size is 128×128 . The cosine annealing learning strategy is applied to adjust the learning rate. The initial learning rate is 2×10^{-4} and decays to 10^{-7} . The period of cosine is 500k iterations. For DASR, we first train the degradation encoder using the same training data

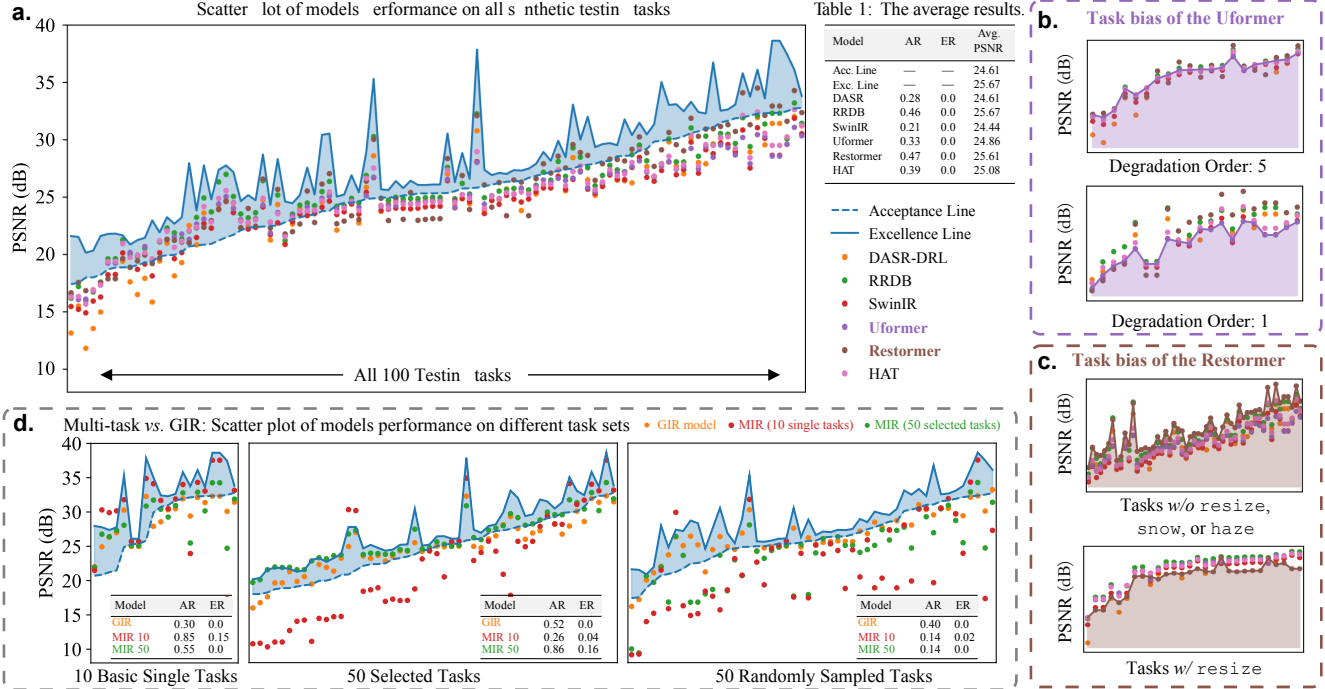


Figure 5: Benchmark results of the existing approaches using the GIR evaluation protocol. (a) shows the scatter plot of models performance on all synthetic testing tasks; (b) shows the task bias of Uformer and (c) shows the task bias of Restormer, please refer to Section 5.3 for more details; (d) shows the performance of MIR-10, MIR-50 and GIR models on different degradations respectively.

and then train the main module following the original paper. All models are built on the PyTorch [80].

5.2. Effectiveness of GIR

In this section, we show the effectiveness and importance of GIR through the quality and quantity results of benchmarked methods. We only use the simplest training strategy without any generalization optimization to train the existing models. Nonetheless, these models demonstrate better visual quality and generalization compared to MIR and progressive single-task results.

Generalization ability. First, we compare the GIR models with multi-task solutions to illustrate the generalization ability of GIR models. This comparison is intended to evaluate the generality \mathcal{G} . We train two multi-task image restoration models “MIR-10” and “MIR-50” for comparison. The MIR-10 and MIR-50 are trained using 10 basic single / 50 representative tasks with the RRDB [106] backbone. Figure 5d shows the performance and AR/ER of MIR-10, MIR-50 and GIR models on different degradations respectively. The GIR model also uses the same RRDB backbone. As can be seen, the MIR-10 model obtains the highest PSNR value on the ten single tasks but performs poorly on almost all the remaining tasks, illustrating

poor generalization performance and generality. The MIR-50 model, similarly, performs well on the fifty selected tasks on which it is trained. The performance also drops dramatically when it is tested on the other fifty randomly generated degradations. It shows that although the MIR models can achieve acceptable results on their training tasks, they can hardly generalize to other similar tasks. Even a simple change in the degradation strength or order can cause the MIR models to fail. But the simple GIR model can achieve better generalization.

Visual Effects. Next, we present visual comparisons between the GIR model and single-task as well as mixture-task models. For the compared models, we first include the RealESRNet [106] as it is known to deal with multiple degradations. Then we use a multi-task image restoration model “MIR-10” for testing. As we include the mixture degradations, we also employ an intuitive solution for testing. “Step-by-step” represents processing images using non-blind models according to certain degradations (*e.g.*, if an image is degraded first by haze and then by blur, the “Step-by-step” solution will first deblur and then dehaze). Without joint training between different non-blind models, this shows how the discrete single-task models handles mixture degradations. We also test the GIR model with the RRDB backbone. Figure 6 shows the visual comparison

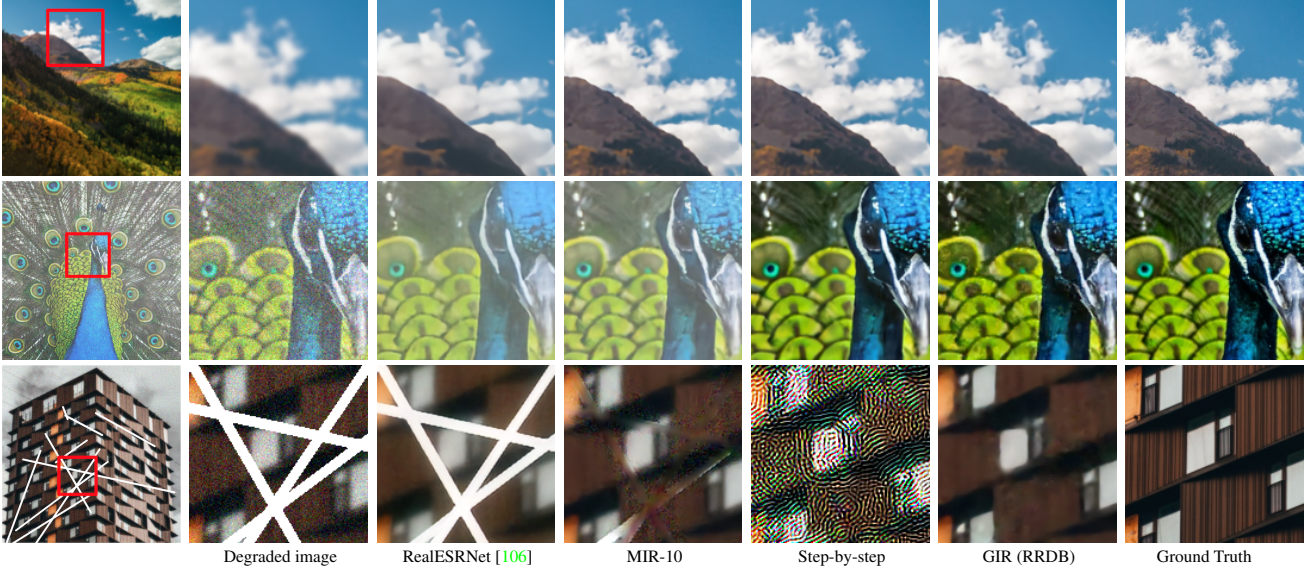


Figure 6: Visual comparison on the presented synthetic testing set. Zoom in for a better view.

of different methods. The first row is a case with a single task `blur`. Almost every model generates good results except that RealESRNet generates over-smooth textures. Individual tasks are generally within the scope of the existing methods. The second row is a mixture case degraded first by haze and then by noise, which can happen in real life. Both RealESRNet and MIR-10 fail in this case. Although MIR-10 was trained with both haze and noise, it only removes noise and cannot deal with this mixture task. The “Step-by-step” can handle such a simple mixture. The third row shows a more complex mixture task, containing damage, noise, ringing, and blur. Due to the accumulated errors and artifacts [116], even if we know the specific degradations, “Step-by-step” still can not produce stable results. Other existing methods unsurprisingly fail. For all the cases, the simple GIR model can output reasonable results.

Real-world cases. Finally, we show the reconstruction results of a real-world image in Figure 7. It focuses on the evaluation of \mathcal{R} . The input image contains observable haze, noise and compression artifacts. The RealESRNet model removes almost all the artifacts but can do nothing for the haze. Compared to the GIR model, the dehaze model has similar dehazing performance but also retains unnatural artifacts and noise. The GIR model not only removes the haze, but also fixes various artifacts in the image. Quantitative results also speak to the same conclusion. The degradations involved in these four test sets in Table 3 have not been extensively studied, so few works can address them simultaneously. We show the results of the deblur and denoise models, as these two degradations are the most com-

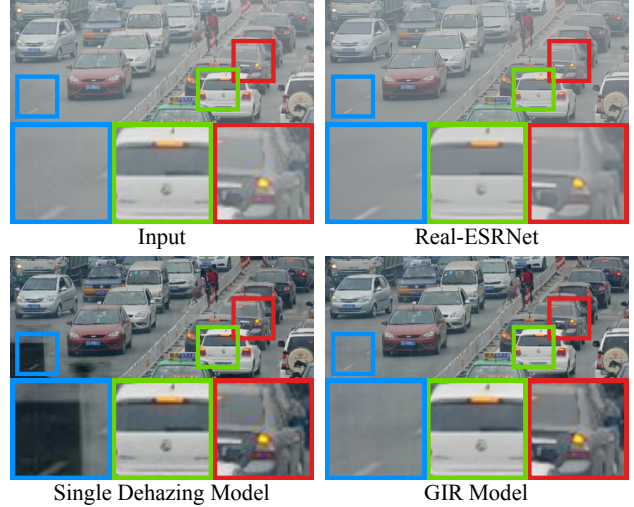


Figure 7: Comparison on the real-world testing image. Zoom in for a better view.

mon ones. Besides that, we also compare our GIR models with RealESRNet. The results illustrate the GIR models can obtain better NIQE values in almost all these datasets.

Significance of GIR. GIR addresses a key limitation observed in previous image restoration studies: generalization. While often overlooked, this aspect is of paramount importance. When juxtaposed with other image restoration methods such as single-task, MIR, and BIR, GIR’s distinctiveness emerges from its encompassing research paradigm. Instead of concentrating on a handful of scenarios, GIR ad-

Real Data	Deblur	Denoise	RealESRNet	GIR
Resize	5.30	6.29	6.03	5.65
Blur	5.96	6.28	6.71	5.68
Noise	6.37	6.14	9.18	5.30
Rain	6.53	6.74	6.45	5.85
Haze	5.71	5.59	6.57	4.87
Snow	5.00	4.79	5.10	4.67
Old film	6.71	6.90	6.72	6.45
Old photo	3.48	3.69	4.71	3.62
Surveillance	6.28	6.58	6.67	6.03
Internet	5.28	5.28	4.85	4.84

Table 3: The NIQE performance of different models on real test sets.

dresses a comprehensive range of situations. Thus, even with simpler models, GIR exhibits applicability across a broader spectrum. The introduction of GIR heralded a fresh perspective in image restoration research. Beyond its academic importance, the advancement of GIR equips users with notable image processing capabilities. This is particularly beneficial for individuals or smaller enterprises that might lack resources for bespoke solutions. GIR’s exploration has industrially invigorated the field in a holistic manner. The aim of this research is not to perfect a single scenario or device but to offer a universally acceptable resolution.

5.3. Practical Difficulties of GIR

Even with all these advantages, GIR still faces many difficulties at the current stage. Although above existing approaches are better than other methods, they are far from the GIR goal. We explore the characteristics of these difficulties in this section.

Model Generality. Although GIR models can solve the mixture task problem to a certain extent, their generality is still involved in our concern. These GIR models’ performance evaluated by the proposed generality protocol (acceptance line and excellence line) are summarized in Figure 5a. The AR, ER, and average PSNR values are shown next to the figure. Overall speaking, these models are far from the ideal GIR model. Most models cannot maintain acceptable performance on most tasks. The model with the best AR is GIR-Restormer. However, it cannot beat a 3-layer-CNN model in more than half of these degradations. Note that the average PSNR values of GIR-RRDB, GIR-Restormer, GIR-Uformer and GIR-HAT have exceeded it of the acceptable performances. This conflict suggests that the new metrics are significant. AR and ER can reflect the model’s generality that the average PSNR cannot describe. Moreover, no existing model can reach the line of excellence in all testing tasks.

Moreover, in this training setting, we found that the

CNN-based model RRDB outperforms some Transformer-based models and comes close to the best model, GIR-Restormer (even surpassing it in average PSNR), despite Transformers generally demonstrating superior performance over CNNs in various single tasks. There are many possible reasons, such as Transformer are poor at GIR or the optimization is inappropriate. We use same learning rate and training iterations for all models but it may be not suitable for each model and degradation. It may also be due to some Transformer models having a preference for specific degradations.

Network Bias. One possible reason for the poor generalization (especially for Transformer methods) may be that different networks have their preferred tasks, although they have the same training settings. This phenomenon has been found in RealSR tasks [130]. We illustrate this using Uformer [109] and Restormer [117]. As illustrated in Figure 5b, the GIR-Uformer (purple) model excels in handling complex degradations but struggles with simpler degradation scenarios. On the other hand, Figure 5c reveals that the GIR-Restormer (brown) exhibits poor performance on almost all degradations involving resize, yet demonstrates impressive capabilities in addressing the remaining tasks. These two Transformer-based models exhibit distinct task-specific preferences that are not observed in SwinIR and HAT. This indicates that future research on the backbone of GIR models should carefully consider task preference to achieve optimal generalization across various tasks. We take a closer look at them in Section 6

Effect of Training Data Scale. General large models are often inseparable from extremely large datasets. However, we question whether this perception holds true for GIR. We investigate the influence of training data scale for GIR models. Table 4a shows that using half or even a quarter of all the training data can still achieve comparable performance. It proves that the core bottleneck of current GIR is not dataset scale. Existing models may not fully utilize even a quarter of the training data with these complex degradations, let alone larger datasets.

A recent study may offer some explanation for this anomaly. Gu et al. [39] found that using fewer images for training may actually lead to better generalization performance in deraining studies. This is because the network tends to choose the simpler task between learning degradation and image content. In most cases, learning degradation is simpler than learning image content. Our results may suggest that a better GIR model should benefit from more training data. It also shows some of the inadequacies of today’s technology.

Surprisingly, adding ImageNet [29] images to the training set decreases the GIR performance. This confirms our conclusion that GIR needs high-quality images for training

ID	Data Scale	AR	ER	Avg. PSNR	ID	Patch size	AR	ER	Avg. PSNR	ID	Batch size	AR	ER	Avg. PSNR
(a)	Quarter of DF2K	0.49	0.0	25.69	(e)	64	0.29	0.0	24.84	(i)	4	0.35	0.0	25.16
(b)	Half of DF2K	0.42	0.0	25.51	(f)	128	0.49	0.0	25.67	(j)	8	0.49	0.0	25.67
(c)	All of DF2K	0.46	0.0	25.67	(g)	192	0.52	0.0	25.95	(k)	16	0.54	0.02	26.00
(d)	ImageNet + DF2K	0.44	0.0	25.38	(h)	256	0.56	0.03	26.21	(l)	32	0.57	0.03	26.39

(a) Ablation study of training data scales.

(b) Ablation study of training patch size.

(c) Ablation study of training batch size.

Table 4: Ablation studies of the factors that might influence the results.

and testing, while the image quality of ImageNet is not desirable, containing noise and compression. Therefore, high-quality training data is still in demand for GIR.

Effect of Training Strategy. We also explore the influence of the training batch and patch size. As shown in Table 4b and Table 4c, we can see that all three metrics are improving with the increasing batch and patch size. However, the marginal effect of this improvement is diminishing. We also find that models with larger batch and patch sizes may achieve the excellence line in some degradations. All these degradations included snow or rain, illustrating that batch and patch sizes may have a greater impact on such degradations. Detailed results are provided in appendix.

6. Interpret GIR Model for Future Direction

The GIR problem emphasizes the ability to generalize. The various models we tested also exhibited different generalization performances. However, apart from the difference in PSNR of the output images, we also want to know what contributes to or hurts the network’s generalization ability. This will inspire future research. Next, we investigate the GIR models through the lens of network interpretation and visualization. In the following experiments, we still focus on the “MIR-10”, “MIR-50” and the GIR model mentioned at the beginning of Section 5.2. We focus on three tasks as our research objectives: The first task is one of the ten basic single tasks and is included in the training set of the MIR-10 and MIR-50 models. The second task is sampled from the fifty representative testing tasks and is in the training set of the MIR-50 model. The last task is randomly generated and not presented in any model’s training set.

Deep Degradation Representation. Liu *et al.* [68] present a concept called deep degradation representation (DDR). Here, we will refer to Figure 8 when introducing DDR. Each point in a subfigure represents an extracted feature from an input image. There are 300 points for every sub-figure. These samples are produced from the above three degradations. Each degradation corresponds to the same 100 images and is marked with the same color. DDR reveals that networks could automatically classify the inputs to different “degradation semantics”. Inputs with similar degradations (points with the same color) will be clustered.

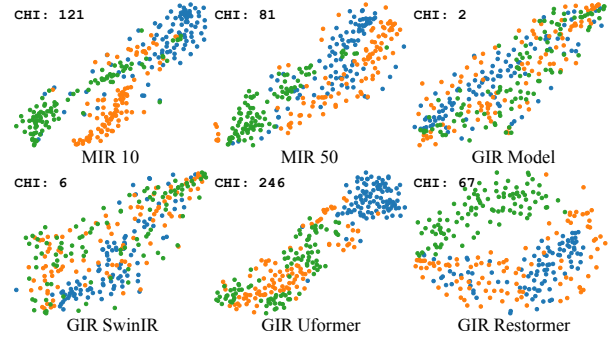


Figure 8: The DDR clustering analysis of different models.

If the obtained clusters are well divided, the network tends to assign different processing strategies for different degradations, resulting in poor generalization performance. Conversely, the network prefers to process degradations similarly and shows stable generality performance. We can use Calinski-Harabaz Index (CHI) [10] to measure the separation degree of clusters. A lower CHI means a weaker clustering degree and indicates a better generalization ability. From the first row of Figure 8, we can observe the relationship between the clustering degrees from the models is MIR-10>MIR-50>GIR model. It also illustrates that GIR models have a better generalization ability.

Besides that, the second row of Figure 8 shows that the Uformer and Restormer tend to divide input samples into clusters, while SwinIR does not show similar behaviour. In this way, Uformer and Restormer may approach GIR by remembering training degradation combinations. This phenomenon is related to their task preferences (See Section 5.3 – they all try to separate individual tasks and optimize them accordingly. This suggests that different networks have different model behaviors and produce different generality effects, even though they are all GIR models. This deserves further study and can help us design better GIR backbone networks.

Attribution analysis. Local attribution map (LAM) [36] is a recent technique that visualizes how the network utilizes information from input pixels. In each row of Figure 9, three LAM maps correspond to MIR-10, MIR-50 and the GIR model, respectively. The heat maps indicate pixels that models utilize to reconstruct the patch marked by a red box.

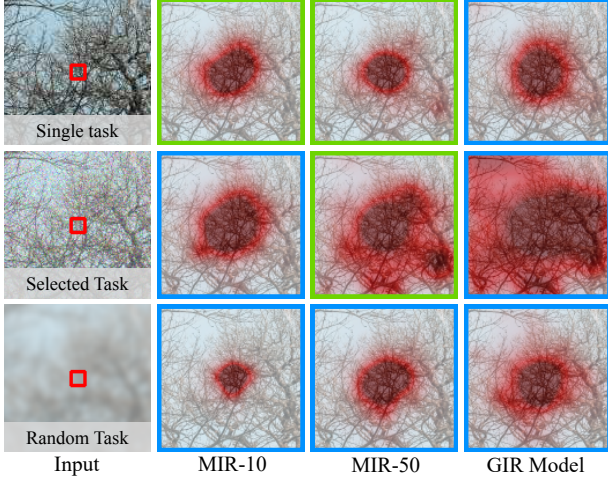


Figure 9: The attribution analysis of different models. Green boxes indicate that the task is explicitly included during model training.

DI values are shown in Table 5. A higher DI represents a wider range of used pixels. We can see the GIR model utilizes the most information when dealing with these tasks. When these models are applied to the single task, all the models can obtain acceptable performance. These models share similar information utilization strategies and DI values. However, the MIR models are increasingly unable to handle mixture degradations. The pixel range used also becomes different between MIR and GIR. MIR can only utilize more information and achieve results similar to those of GIR when faced with tasks that appeared during training (green boxes). Compared to MIR, GIR models can directly utilize more information from the input, especially in unseen complex mixture tasks.

Degradation Cases	MIR-10		MIR-50		GIR Model	
	DI	PSNR	DI	PSNR	DI	PSNR
Single Task	8.7	32.37	9.2	31.37	11.3	30.79
Mixture Selected Task	17.8	12.86	20.5	24.8	22.4	22.73
Randomly Generated Task	7.9	10.53	14.4	10.90	18.2	19.99

Table 5: The Diffusion Index of different test cases. Green boxes indicate that the task is explicitly included during model training.

7. Conclusion

In this work, we present a new problem called general image restoration. We have established a research framework for GIR, including its definition, dataset, and evaluation metrics, and conducted a preliminary exploration. Our discussions demonstrate that GIR is of practical and theoretical importance. We hope our work can lay the foundation

towards a real general model in image restoration.

Authors’ Note. Initially drafted in 2022, this work represents a major step toward achieving low-level vision intelligence and generalization. Since 2022, the development of language [85, 86, 6, 98, 99] and multimodal models [84, 63, 62] has introduced new paradigms for general intelligence. The widespread application of diffusion models [44, 91] has brought new vitality to low-level vision advancements [103, 59, 112, 115, 110]. However, even two years later, the insights provided by this paper on general image restoration remain highly valuable.

We believe that general image restoration revolves around three critical aspects: generalization, unification, and intelligence. The primary focus of this paper is on the issue of generalization. We have developed a systematic evaluation method to quantify the generalization capability of general image restoration models, which we consider fundamental to the problem. Unification emphasizes that general image restoration should be achieved through a unified system rather than breaking the problem into smaller, independent tasks. Intelligence represents the deeper requirements of general intelligence for model performance. For example, a possible form of intelligent image restoration is that models have a better understanding of natural images space, thus they can remove degradation by removing unreasonable parts of the natural image space.

Over the past two years, large language models [85, 98], multimodal language models [84, 63], and diffusion models [44, 91] have each interpreted these three aspects in their respective domains. Multimodal language models introduce explicit intelligence driven by language, while diffusion models, based on generative priors, offer inspiration for addressing generalization issues. The pursuit of large-scale models [2, 93, 9] has made it possible to develop a comprehensive, universal model. SUPIR [115] is a product of this developmental path. SUPIR erases the degradation and parts of details to produce a “blurry input”, and then executes conditional generation based on it. Although SUPIR utilizes powerful priors to greatly improve the visual effect of restoration, it does not solve the generalization problem of degradation outside the training set.

General image restoration points toward a research direction focused on developing unified, generalizable, and intelligent image restoration models. However, this direction still faces challenges related to generalization and intelligence, which will be central issues in future image restoration research.

References

- [1] Abdelrahman Abdelhamed, Stephen Lin, and Michael S Brown. A high-quality denoising dataset for smartphone cameras. In *Proceedings of the IEEE Conference on Computer Vision and Pattern Recognition*, pages 1692–1700, 2018. 2, 3, 7, 19

- [2] Josh Achiam, Steven Adler, Sandhini Agarwal, Lama Ahmad, Ilge Akkaya, Florencia Leoni Aleman, Diogo Almeida, Janko Altmerschmidt, Sam Altman, Shyamal Anadkat, et al. Gpt-4 technical report. *arXiv preprint arXiv:2303.08774*, 2023. 13
- [3] Eirikur Agustsson and Radu Timofte. Ntire 2017 challenge on single image super-resolution: Dataset and study. In *Proceedings of the IEEE Conference on Computer Vision and Pattern Recognition (CVPR) Workshops*, July 2017. 8, 20
- [4] Hangbo Bao, Li Dong, and Furu Wei. Beit: Bert pre-training of image transformers. *arXiv preprint arXiv:2106.08254*, 2021. 3
- [5] Marcelo Bertalmio, Guillermo Sapiro, Vincent Caselles, and Coloma Ballester. Image inpainting. In *Proceedings of the 27th annual conference on Computer graphics and interactive techniques*, pages 417–424, 2000. 19
- [6] Tom Brown, Benjamin Mann, Nick Ryder, Melanie Subbiah, Jared D Kaplan, Prafulla Dhariwal, Arvind Neelakantan, Pranav Shyam, Girish Sastry, Amanda Askell, et al. Language models are few-shot learners. *Advances in neural information processing systems*, 33:1877–1901, 2020. 3, 13
- [7] Bolun Cai, Xiangmin Xu, Kui Jia, Chunmei Qing, and Dacheng Tao. Dehazenet: An end-to-end system for single image haze removal. *IEEE Transactions on Image Processing*, 25(11):5187–5198, 2016. 2
- [8] Jianrui Cai, Hui Zeng, Hongwei Yong, Zisheng Cao, and Lei Zhang. Toward real-world single image super-resolution: A new benchmark and a new model. In *Proceedings of the IEEE International Conference on Computer Vision*, 2019. 3, 7
- [9] Zheng Cai, Maosong Cao, Haojiong Chen, Kai Chen, Keyu Chen, Xin Chen, Xun Chen, Zehui Chen, Zhi Chen, Pei Chu, et al. Internlm2 technical report. *arXiv preprint arXiv:2403.17297*, 2024. 13
- [10] Tadeusz Caliński and Jerzy Harabasz. A dendrite method for cluster analysis. *Communications in Statistics-theory and Methods*, 3(1):1–27, 1974. 12
- [11] Mathilde Caron, Hugo Touvron, Ishan Misra, Hervé Jégou, Julien Mairal, Piotr Bojanowski, and Armand Joulin. Emerging properties in self-supervised vision transformers. In *Proceedings of the IEEE/CVF International Conference on Computer Vision*, pages 9650–9660, 2021. 3
- [12] Haoyu Chen, Jinjin Gu, Yihao Liu, Salma Abdel Magid, Chao Dong, Qiong Wang, Hanspeter Pfister, and Lei Zhu. Masked image training for generalizable deep image denoising. In *Proceedings of the IEEE/CVF Conference on Computer Vision and Pattern Recognition*, pages 1692–1703, 2023. 2, 3
- [13] Hanting Chen, Yunhe Wang, Tianyu Guo, Chang Xu, Yiping Deng, Zhenhua Liu, Siwei Ma, Chunjing Xu, Chao Xu, and Wen Gao. Pre-trained image processing transformer. In *Proceedings of the IEEE/CVF Conference on Computer Vision and Pattern Recognition*, pages 12299–12310, 2021. 3, 8
- [14] Liangyu Chen, Xiaojie Chu, Xiangyu Zhang, and Jian Sun. Simple baselines for image restoration. *arXiv preprint arXiv:2204.04676*, 2022. 1
- [15] Liangyu Chen, Xin Lu, Jie Zhang, Xiaojie Chu, and Chengpeng Chen. Hinet: Half instance normalization network for image restoration. In *Proceedings of the IEEE/CVF Conference on Computer Vision and Pattern Recognition*, pages 182–192, 2021. 2
- [16] Ting Chen, Simon Kornblith, Mohammad Norouzi, and Geoffrey Hinton. A simple framework for contrastive learning of visual representations. In *International conference on machine learning*, pages 1597–1607. PMLR, 2020. 3
- [17] Wei-Ting Chen, Hao-Yu Fang, Cheng-Lin Hsieh, Cheng-Che Tsai, I Chen, Jian-Jiun Ding, Sy-Yen Kuo, et al. All snow removed: Single image desnowing algorithm using hierarchical dual-tree complex wavelet representation and contradict channel loss. In *Proceedings of the IEEE/CVF International Conference on Computer Vision*, pages 4196–4205, 2021. 2, 20
- [18] Wei-Ting Chen, Zhi-Kai Huang, Cheng-Che Tsai, Hao-Hsiang Yang, Jian-Jiun Ding, and Sy-Yen Kuo. Learning multiple adverse weather removal via two-stage knowledge learning and multi-contrastive regularization: Toward a unified model. 2022. 3
- [19] Xinlei Chen and Kaiming He. Exploring simple siamese representation learning. In *Proceedings of the IEEE/CVF Conference on Computer Vision and Pattern Recognition*, pages 15750–15758, 2021. 3
- [20] Xiangyu Chen, Zheyuan Li, Yuandong Pu, Yihao Liu, Jiantao Zhou, Yu Qiao, and Chao Dong. A comparative study of image restoration networks for general backbone network design. *arXiv preprint arXiv:2310.11881*, 2023. 3
- [21] Xiangyu Chen, Yihao Liu, Yuandong Pu, Wenlong Zhang, Jiantao Zhou, Yu Qiao, and Chao Dong. Learning a low-level vision generalist via visual task prompt. *arXiv preprint arXiv:2408.08601*, 2024. 2, 3
- [22] Xiangyu Chen, Xintao Wang, Jiantao Zhou, and Chao Dong. Activating more pixels in image super-resolution transformer. *arXiv preprint arXiv:2205.04437*, 2022. 1, 8
- [23] Xinlei Chen, Saining Xie, and Kaiming He. An empirical study of training self-supervised vision transformers. In *Proceedings of the IEEE/CVF International Conference on Computer Vision*, pages 9640–9649, 2021. 3
- [24] Zheng Chen, Yulun Zhang, Jinjin Gu, Linghe Kong, Xiaokang Yang, and Fisher Yu. Dual aggregation transformer for image super-resolution. In *Proceedings of the IEEE international conference on computer vision*, 2023. 1
- [25] X Chu, L Chen, C Chen, and X Lu. Improving image restoration by revisiting global information aggregation. *arXiv preprint arXiv:2112.04491*, 5, 2021. 1
- [26] Zihang Dai, Hanxiao Liu, Quoc V Le, and Mingxing Tan. Coatnet: Marrying convolution and attention for all data sizes. *Advances in Neural Information Processing Systems*, 34:3965–3977, 2021. 3
- [27] Unsplash Dataset. Unsplash dataset. <https://unsplash.com/data>. 6
- [28] Jia Deng, Wei Dong, Richard Socher, Li-Jia Li, Kai Li, and Li Fei-Fei. Imagenet: A large-scale hierarchical image database. In *2009 IEEE conference on computer vision and pattern recognition*, pages 248–255. Ieee, 2009. 3

- [29] Jia Deng, Wei Dong, Richard Socher, Li-Jia Li, Kai Li, and Li Fei-Fei. Imagenet: A large-scale hierarchical image database. In *2009 IEEE conference on computer vision and pattern recognition*, pages 248–255. Ieee, 2009. 11, 20
- [30] Chao Dong, Yubin Deng, Chen Change Loy, and Xiaoou Tang. Compression artifacts reduction by a deep convolutional network. In *Proceedings of the IEEE international conference on computer vision*, pages 576–584, 2015. 2
- [31] Chao Dong, Chen Change Loy, Kaiming He, and Xiaoou Tang. Image super-resolution using deep convolutional networks. *IEEE transactions on pattern analysis and machine intelligence*, 38(2):295–307, 2015. 2, 7, 19
- [32] Jiangxin Dong and Jinshan Pan. Physics-based feature dehazing networks. In *European Conference on Computer Vision*, pages 188–204. Springer, 2020. 2
- [33] Xueyang Fu, Jiabin Huang, Xinghao Ding, Yinghao Liao, and John Paisley. Clearing the skies: A deep network architecture for single-image rain removal. *IEEE Transactions on Image Processing*, 26(6):2944–2956, 2017. 2, 19
- [34] Priya Goyal, Quentin Duval, Isaac Seessel, Mathilde Caron, Ishan Misra, Levent Sagun, Armand Joulin, and Piotr Bojanowski. Vision Models Are More Robust And Fair When Pretrained On Uncurated Images Without Supervision. *arXiv e-prints*, page arXiv:2202.08360, Feb. 2022. 3
- [35] Jean-Bastien Grill, Florian Strub, Florent Altché, Corentin Tallec, Pierre Richemond, Elena Buchatskaya, Carl Doersch, Bernardo Avila Pires, Zhaohan Guo, Mohammad Gheshlaghi Azar, et al. Bootstrap your own latent-a new approach to self-supervised learning. *Advances in neural information processing systems*, 33:21271–21284, 2020. 3
- [36] Jinjin Gu and Chao Dong. Interpreting super-resolution networks with local attribution maps. In *Proceedings of the IEEE/CVF Conference on Computer Vision and Pattern Recognition*, pages 9199–9208, 2021. 2, 12
- [37] Jinjin Gu, Hannan Lu, Wangmeng Zuo, and Chao Dong. Blind super-resolution with iterative kernel correction. In *Proceedings of the IEEE/CVF Conference on Computer Vision and Pattern Recognition*, pages 1604–1613, 2019. 2, 3
- [38] Jinjin Gu, Hannan Lu, Wangmeng Zuo, and Chao Dong. Blind super-resolution with iterative kernel correction. In *Proceedings of the IEEE/CVF Conference on Computer Vision and Pattern Recognition*, pages 1604–1613, 2019. 4
- [39] Jinjin Gu, Xianzheng Ma, Xiangtao Kong, Yu Qiao, and Chao Dong. Networks are slacking off: Understanding generalization problem in image deraining. *arXiv preprint arXiv:2305.15134*, 2023. 1, 2, 3, 11
- [40] Jingwen He, Chao Dong, and Yu Qiao. Modulating image restoration with continual levels via adaptive feature modification layers. In *Proceedings of the IEEE/CVF Conference on Computer Vision and Pattern Recognition*, pages 11056–11064, 2019. 8
- [41] Jingwen He, Chao Dong, Liu Yihao, and Yu Qiao. Interactive multi-dimension modulation for image restoration. *IEEE Transactions on Pattern Analysis and Machine Intelligence*, 2021. 8
- [42] Kaiming He, Xinlei Chen, Saining Xie, Yanghao Li, Piotr Dollár, and Ross Girshick. Masked autoencoders are scalable vision learners. In *Proceedings of the IEEE/CVF Conference on Computer Vision and Pattern Recognition*, pages 16000–16009, 2022. 3
- [43] Kaiming He, Xiangyu Zhang, Shaoqing Ren, and Jian Sun. Deep residual learning for image recognition. In *Proceedings of the IEEE Conference on Computer Vision and Pattern Recognition (CVPR)*, June 2016. 7
- [44] Jonathan Ho, Ajay Jain, and Pieter Abbeel. Denoising diffusion probabilistic models. *Advances in neural information processing systems*, 33:6840–6851, 2020. 13
- [45] Yuqi Huo, Manli Zhang, Guangzhen Liu, Haoyu Lu, Yizhao Gao, Guoxing Yang, Jingyuan Wen, Heng Zhang, Baogui Xu, Weihao Zheng, et al. Wenlan: Bridging vision and language by large-scale multi-modal pre-training. *arXiv preprint arXiv:2103.06561*, 2021. 3
- [46] Jacob Devlin Ming-Wei Chang Kenton and Lee Kristina Toutanova. Bert: Pre-training of deep bidirectional transformers for language understanding. In *Proceedings of NAACL-HLT*, pages 4171–4186, 2019. 3
- [47] Diederik P Kingma and Jimmy Ba. Adam: A method for stochastic optimization. *arXiv preprint arXiv:1412.6980*, 2014. 8
- [48] Xiangtao Kong, Chao Dong, and Lei Zhang. Towards effective multiple-in-one image restoration: A sequential and prompt learning strategy. *arXiv preprint arXiv:2401.03379*, 2024. 3, 5
- [49] Xiangtao Kong, Xina Liu, Jinjin Gu, Yu Qiao, and Chao Dong. Reflash dropout in image super-resolution. In *Proceedings of the IEEE/CVF Conference on Computer Vision and Pattern Recognition*, pages 6002–6012, 2022. 1, 2, 3, 7, 8
- [50] Orest Kupyn, Volodymyr Budzan, Mykola Mykhailych, Dmytro Mishkin, and Jiří Matas. Deblurgan: Blind motion deblurring using conditional adversarial networks. In *Proceedings of the IEEE conference on computer vision and pattern recognition*, pages 8183–8192, 2018. 2
- [51] Christian Ledig, Lucas Theis, Ferenc Huszár, Jose Caballero, Andrew Cunningham, Alejandro Acosta, Andrew Aitken, Alykhan Tejani, Johannes Totz, Zehan Wang, et al. Photo-realistic single image super-resolution using a generative adversarial network. In *Proceedings of the IEEE conference on computer vision and pattern recognition*, pages 4681–4690, 2017. 2
- [52] Boyun Li, Xiao Liu, Peng Hu, Zhongqin Wu, Jiancheng Lv, and Xi Peng. All-In-One Image Restoration for Unknown Corruption. In *IEEE Conference on Computer Vision and Pattern Recognition*, New Orleans, LA, June 2022. 5, 8
- [53] Boyi Li, Wenqi Ren, Dengpan Fu, Dacheng Tao, Dan Feng, Wenjun Zeng, and Zhangyang Wang. Benchmarking single-image dehazing and beyond. *IEEE Transactions on Image Processing*, 28(1):492–505, 2019. 2, 5, 7, 19, 20
- [54] Wenbo Li, Xin Lu, Jiangbo Lu, Xiangyu Zhang, and Jiaya Jia. On efficient transformer and image pre-training for low-level vision. *arXiv preprint arXiv:2112.10175*, 2021. 3, 8
- [55] Zilong Li, Yiming Lei, Chenglong Ma, Junping Zhang, and Hongming Shan. Prompt-in-prompt learning for universal image restoration. *arXiv preprint arXiv:2312.05038*, 2023. 3

- [56] Jingyun Liang, Jiezhong Cao, Guolei Sun, Kai Zhang, Luc Van Gool, and Radu Timofte. Swinir: Image restoration using swin transformer. In *IEEE International Conference on Computer Vision Workshops*, 2021. 8
- [57] Jie Liang, Hui Zeng, and Lei Zhang. Efficient and degradation-adaptive network for real-world image super-resolution. In *European Conference on Computer Vision*, pages 574–591. Springer, 2022. 7
- [58] Bee Lim, Sanghyun Son, Heewon Kim, Seungjun Nah, and Kyoung Mu Lee. Enhanced deep residual networks for single image super-resolution. In *The IEEE Conference on Computer Vision and Pattern Recognition (CVPR) Workshops*, July 2017. 2
- [59] Xinqi Lin, Jingwen He, Ziyang Chen, Zhaoyang Lyu, Ben Fei, Bo Dai, Wanli Ouyang, Yu Qiao, and Chao Dong. Diffbir: Towards blind image restoration with generative diffusion prior. *arXiv preprint arXiv:2308.15070*, 2023. 13
- [60] Anran Liu, Yihao Liu, Jinjin Gu, Yu Qiao, and Chao Dong. Blind image super-resolution: A survey and beyond. *IEEE Transactions on Pattern Analysis and Machine Intelligence*, 2022. 2, 3
- [61] Fayao Liu, Chunhua Shen, Guosheng Lin, and Ian Reid. Learning depth from single monocular images using deep convolutional neural fields. *IEEE Transactions on Pattern Analysis and Machine Intelligence*, 38(10):2024–2039, 2016. 20
- [62] Haotian Liu, Chunyuan Li, Yuheng Li, and Yong Jae Lee. Improved baselines with visual instruction tuning. In *Proceedings of the IEEE/CVF Conference on Computer Vision and Pattern Recognition*, pages 26296–26306, 2024. 13
- [63] Haotian Liu, Chunyuan Li, Qingyang Wu, and Yong Jae Lee. Visual instruction tuning. *Advances in neural information processing systems*, 36, 2024. 13
- [64] Lin Liu, Lingxi Xie, Xiaopeng Zhang, Shanxin Yuan, Xiangyu Chen, Wengang Zhou, Houqiang Li, and Qi Tian. Tape: Task-agnostic prior embedding for image restoration. In *European Conference on Computer Vision*, pages 447–464. Springer, 2022. 3, 5
- [65] Xiaohong Liu, Yongrui Ma, Zhihao Shi, and Jun Chen. Griddehazenet: Attention-based multi-scale network for image dehazing. In *Proceedings of the IEEE/CVF international conference on computer vision*, pages 7314–7323, 2019. 2
- [66] Yihao Liu, Xiangyu Chen, Xianzheng Ma, Xintao Wang, Jiantao Zhou, Yu Qiao, and Chao Dong. Unifying image processing as visual prompting question answering. *arXiv preprint arXiv:2310.10513*, 2023. 2, 3
- [67] Yihao Liu, Jingwen He, Jinjin Gu, Xiangtao Kong, Yu Qiao, and Chao Dong. Degae: A new pretraining paradigm for low-level vision. In *Proceedings of the IEEE/CVF Conference on Computer Vision and Pattern Recognition*, pages 23292–23303, 2023. 3, 8
- [68] Yihao Liu, Anran Liu, Jinjin Gu, Zhipeng Zhang, Wenhao Wu, Yu Qiao, and Chao Dong. Discovering “semantics” in super-resolution networks. *arXiv preprint arXiv:2108.00406*, 2021. 2, 3, 12
- [69] Yihao Liu, Hengyuan Zhao, Jinjin Gu, Yu Qiao, and Chao Dong. Evaluating the generalization ability of super-resolution networks. *arXiv preprint arXiv:2205.07019*, 2022. 1, 3
- [70] Yun-Fu Liu, Da-Wei Jaw, Shih-Chia Huang, and Jenq-Neng Hwang. Desnownet: Context-aware deep network for snow removal. *IEEE Transactions on Image Processing*, 27(6):3064–3073, 2018. 2
- [71] Yun-Fu Liu, Da-Wei Jaw, Shih-Chia Huang, and Jenq-Neng Hwang. Desnownet: Context-aware deep network for snow removal. *IEEE Transactions on Image Processing*, 27(6):3064–3073, 2018. 7
- [72] Michael R Lomnitz. Diffjpeg. <https://github.com/mlomnitz/DiffJPEG>, 2021. 2
- [73] Leon B Lucy. An iterative technique for the rectification of observed distributions. *Astronomical Journal*, Vol. 79, p. 745 (1974), 79:745, 1974. 19
- [74] Zhengxiong Luo, Yan Huang, Shang Li, Liang Wang, and Tieniu Tan. Unfolding the alternating optimization for blind super resolution. *arXiv preprint arXiv:2010.02631*, 2020. 4
- [75] Zhengxiong Luo, Yan Huang, Shang Li, Liang Wang, and Tieniu Tan. End-to-end alternating optimization for blind super resolution, 2021. 4
- [76] Jiaqi Ma, Tianheng Cheng, Guoli Wang, Qian Zhang, Xinggang Wang, and Lefei Zhang. Prores: Exploring degradation-aware visual prompt for universal image restoration. *arXiv preprint arXiv:2306.13653*, 2023. 3
- [77] Yiqun Mei, Yuchen Fan, and Yuqian Zhou. Image super-resolution with non-local sparse attention. In *Proceedings of the IEEE/CVF Conference on Computer Vision and Pattern Recognition*, pages 3517–3526, 2021. 2
- [78] Seungjun Nah, Tae Hyun Kim, and Kyoung Mu Lee. Deep multi-scale convolutional neural network for dynamic scene deblurring. In *Proceedings of the IEEE conference on computer vision and pattern recognition*, pages 3883–3891, 2017. 7
- [79] Andrew Ng, Michael Jordan, and Yair Weiss. On spectral clustering: Analysis and an algorithm. *Advances in neural information processing systems*, 14, 2001. 7, 20
- [80] Adam Paszke, Sam Gross, Soumith Chintala, Gregory Chanan, Edward Yang, Zachary DeVito, Zeming Lin, Alban Desmaison, Luca Antiga, and Adam Lerer. Automatic differentiation in pytorch. 2017. 9
- [81] Deepak Pathak, Philipp Krahenbuhl, Jeff Donahue, Trevor Darrell, and Alexei A Efros. Context encoders: Feature learning by inpainting. In *Proceedings of the IEEE conference on computer vision and pattern recognition*, pages 2536–2544, 2016. 2
- [82] Vaishnav Potlapalli, Syed Waqas Zamir, Salman Khan, and Fahad Shahbaz Khan. Promptir: Prompting for all-in-one blind image restoration. *Advances in Neural Information Processing Systems (NeurIPS)*, 2023. 3
- [83] Alec Radford, Jong Wook Kim, Chris Hallacy, Aditya Ramesh, Gabriel Goh, Sandhini Agarwal, Girish Sastry, Amanda Askell, Pamela Mishkin, Jack Clark, et al. Learning transferable visual models from natural language supervision. In *International Conference on Machine Learning*, pages 8748–8763. PMLR, 2021. 3
- [84] Alec Radford, Jong Wook Kim, Chris Hallacy, Aditya Ramesh, Gabriel Goh, Sandhini Agarwal, Girish Sastry, Amanda Askell, Pamela Mishkin, Jack Clark, Gretchen Krueger, and Ilya Sutskever. Learning Transferable Visual Models From Natural Language Supervision. *arXiv e-prints*, page arXiv:2103.00020, Feb. 2021. 3, 13

- [85] Alec Radford, Karthik Narasimhan, Tim Salimans, Ilya Sutskever, et al. Improving language understanding by generative pre-training. 2018. [13](#)
- [86] Alec Radford, Jeffrey Wu, Rewon Child, David Luan, Dario Amodei, Ilya Sutskever, et al. Language models are unsupervised multitask learners. *OpenAI blog*, 1(8):9, 2019. [13](#)
- [87] Dongwei Ren, Wangmeng Zuo, Qinghua Hu, Pengfei Zhu, and Deyu Meng. Progressive image deraining networks: A better and simpler baseline. In *Proceedings of the IEEE/CVF Conference on Computer Vision and Pattern Recognition*, pages 3937–3946, 2019. [2](#)
- [88] William Hadley Richardson. Bayesian-Based Iterative Method of Image Restoration. *Journal of the Optical Society of America (1917-1983)*, 62(1):55, Jan. 1972. [19](#)
- [89] Jaesung Rim, Haeyun Lee, Jucheol Won, and Sunghyun Cho. Real-world blur dataset for learning and benchmarking deblurring algorithms. In *European Conference on Computer Vision*, pages 184–201. Springer, 2020. [7](#)
- [90] Carlos Riquelme, Joan Puigcerver, Basil Mustafa, Maxim Neumann, Rodolphe Jenatton, André Susano Pinto, Daniel Keysers, and Neil Houlsby. Scaling vision with sparse mixture of experts. *Advances in Neural Information Processing Systems*, 34:8583–8595, 2021. [3](#)
- [91] Robin Rombach, Andreas Blattmann, Dominik Lorenz, Patrick Esser, and Björn Ommer. High-resolution image synthesis with latent diffusion models. In *Proceedings of the IEEE/CVF conference on computer vision and pattern recognition*, pages 10684–10695, 2022. [13](#)
- [92] Ozan Sener and Vladlen Koltun. Multi-task learning as multi-objective optimization. *Advances in neural information processing systems*, 31, 2018. [4](#)
- [93] Jing Shao, Siyu Chen, Yangguang Li, Kun Wang, Zhenfei Yin, Yanan He, Jianing Teng, Qinghong Sun, Mengya Gao, Jihao Liu, et al. Intern: A new learning paradigm towards general vision. *arXiv preprint arXiv:2111.08687*, 2021. [1](#), [3](#), [13](#)
- [94] Yuda Song, Zhuqing He, Hui Qian, and Xin Du. Vision transformers for single image dehazing. *arXiv preprint arXiv:2204.03883*, 2022. [2](#)
- [95] Chen Sun, Abhinav Shrivastava, Saurabh Singh, and Abhinav Gupta. Revisiting unreasonable effectiveness of data in deep learning era. In *Proceedings of the IEEE international conference on computer vision*, pages 843–852, 2017. [3](#)
- [96] Xin Tao, Hongyun Gao, Xiaoyong Shen, Jue Wang, and Jiaya Jia. Scale-recurrent network for deep image deblurring. In *Proceedings of the IEEE conference on computer vision and pattern recognition*, pages 8174–8182, 2018. [2](#)
- [97] Radu Timofte, Eirikur Agustsson, Luc Van Gool, Ming-Hsuan Yang, and Lei Zhang. Ntire 2017 challenge on single image super-resolution: Methods and results. In *Proceedings of the IEEE conference on computer vision and pattern recognition workshops*, pages 114–125, 2017. [8](#), [20](#)
- [98] Hugo Touvron, Thibaut Lavril, Gautier Izacard, Xavier Martinet, Marie-Anne Lachaux, Timothée Lacroix, Baptiste Rozière, Naman Goyal, Eric Hambro, Faisal Azhar, et al. Llama: Open and efficient foundation language models. *arXiv preprint arXiv:2302.13971*, 2023. [13](#)
- [99] Hugo Touvron, Louis Martin, Kevin Stone, Peter Albert, Amjad Almahairi, Yasmine Babaei, Nikolay Bashlykov, Soumya Batra, Prajjwal Bhargava, Shrutie Bhosale, et al. Llama 2: Open foundation and fine-tuned chat models. *arXiv preprint arXiv:2307.09288*, 2023. [13](#)
- [100] Ulrike Von Luxburg. A tutorial on spectral clustering. *Statistics and computing*, 17(4):395–416, 2007. [7](#), [20](#)
- [101] Ziyu Wan, Bo Zhang, Dongdong Chen, Pan Zhang, Dong Chen, Jing Liao, and Fang Wen. Bringing old photos back to life. In *proceedings of the IEEE/CVF conference on computer vision and pattern recognition*, pages 2747–2757, 2020. [7](#)
- [102] Hong Wang, Zongsheng Yue, Qi Xie, Qian Zhao, Yefeng Zheng, and Deyu Meng. From rain generation to rain removal. In *Proceedings of the IEEE/CVF Conference on Computer Vision and Pattern Recognition*, pages 14791–14801, 2021. [19](#)
- [103] Jianyi Wang, Zongsheng Yue, Shangchen Zhou, Kelvin CK Chan, and Chen Change Loy. Exploiting diffusion prior for real-world image super-resolution. *International Journal of Computer Vision*, pages 1–21, 2024. [13](#)
- [104] Longguang Wang, Yingqian Wang, Xiaoyu Dong, Qingyu Xu, Jungang Yang, Wei An, and Yulan Guo. Unsupervised degradation representation learning for blind super-resolution. In *CVPR*, 2021. [8](#)
- [105] Tianyu Wang, Xin Yang, Ke Xu, Shaozhe Chen, Qiang Zhang, and Rynson WH Lau. Spatial attentive single-image deraining with a high quality real rain dataset. In *Proceedings of the IEEE/CVF Conference on Computer Vision and Pattern Recognition*, pages 12270–12279, 2019. [7](#)
- [106] Xintao Wang, Liangbin Xie, Chao Dong, and Ying Shan. Real-esrgan: Training real-world blind super-resolution with pure synthetic data. In *International Conference on Computer Vision Workshops (ICCVW)*, 2021. [1](#), [3](#), [6](#), [8](#), [9](#), [10](#), [19](#)
- [107] Xintao Wang, Ke Yu, Shixiang Wu, Jinjin Gu, Yihao Liu, Chao Dong, Yu Qiao, and Chen Change Loy. Esrgan: Enhanced super-resolution generative adversarial networks. In *Proceedings of the European Conference on Computer Vision (ECCV)*, pages 0–0, 2018. [8](#)
- [108] Zhou Wang, Alan C Bovik, Hamid R Sheikh, and Eero P Simoncelli. Image quality assessment: from error visibility to structural similarity. *IEEE transactions on image processing*, 13(4):600–612, 2004. [8](#)
- [109] Zhendong Wang, Xiaodong Cun, Jianmin Bao, Wengang Zhou, Jianzhuang Liu, and Houqiang Li. Uformer: A general u-shaped transformer for image restoration. In *Proceedings of the IEEE/CVF Conference on Computer Vision and Pattern Recognition*, pages 17683–17693, 2022. [8](#), [11](#)
- [110] Rongyuan Wu, Tao Yang, Lingchen Sun, Zhengqiang Zhang, Shuai Li, and Lei Zhang. Seesr: Towards semantics-aware real-world image super-resolution. In *Proceedings of the IEEE/CVF conference on computer vision and pattern recognition*, pages 25456–25467, 2024. [13](#)
- [111] Yi Wu, Jongwoo Lim, and Ming-Hsuan Yang. Online object tracking: A benchmark. In *IEEE Conference on Computer Vision and Pattern Recognition (CVPR)*, 2013. [7](#)
- [112] Tao Yang, Rongyuan Wu, Peiran Ren, Xuansong Xie, and Lei Zhang. Pixel-aware stable diffusion for realistic im-

- age super-resolution and personalized stylization. *arXiv preprint arXiv:2308.14469*, 2023. 13
- [113] Wenhan Yang, Robby T Tan, Jiashi Feng, Jiaying Liu, Zongming Guo, and Shuicheng Yan. Deep joint rain detection and removal from a single image. In *Proceedings of the IEEE conference on computer vision and pattern recognition*, pages 1357–1366, 2017. 2
 - [114] Wenhan Yang, Robby T Tan, Jiashi Feng, Jiaying Liu, Zongming Guo, and Shuicheng Yan. Deep joint rain detection and removal from a single image. In *Proceedings of the IEEE conference on computer vision and pattern recognition*, pages 1357–1366, 2017. 2, 3, 19
 - [115] Fanghua Yu, Jinjin Gu, Zheyuan Li, Jinfan Hu, Xiangtao Kong, Xintao Wang, Jingwen He, Yu Qiao, and Chao Dong. Scaling up to excellence: Practicing model scaling for photo-realistic image restoration in the wild. In *Proceedings of the IEEE/CVF Conference on Computer Vision and Pattern Recognition*, pages 25669–25680, 2024. 13
 - [116] Ke Yu, Xintao Wang, Chao Dong, Xiaoou Tang, and Chen Change Loy. Path-restore: Learning network path selection for image restoration. *arXiv preprint arXiv:1904.10343*, 2019. 10
 - [117] Syed Waqas Zamir, Aditya Arora, Salman Khan, Munawar Hayat, Fahad Shahbaz Khan, and Ming-Hsuan Yang. Restormer: Efficient transformer for high-resolution image restoration. In *Proceedings of the IEEE/CVF Conference on Computer Vision and Pattern Recognition*, pages 5728–5739, 2022. 8, 11
 - [118] Syed Waqas Zamir, Aditya Arora, Salman Khan, Munawar Hayat, Fahad Shahbaz Khan, Ming-Hsuan Yang, and Ling Shao. Multi-stage progressive image restoration. In *Proceedings of the IEEE/CVF conference on computer vision and pattern recognition*, pages 14821–14831, 2021. 2
 - [119] Xiaohua Zhai, Alexander Kolesnikov, Neil Houlsby, and Lucas Beyer. Scaling vision transformers. In *Proceedings of the IEEE/CVF Conference on Computer Vision and Pattern Recognition*, pages 12104–12113, 2022. 3
 - [120] Xiaohua Zhai, Alexander Kolesnikov, Neil Houlsby, and Lucas Beyer. Scaling vision transformers. In *Proceedings of the IEEE/CVF Conference on Computer Vision and Pattern Recognition (CVPR)*, pages 12104–12113, June 2022. 3
 - [121] He Zhang and Vishal M Patel. Density-aware single image de-raining using a multi-stream dense network. In *Proceedings of the IEEE conference on computer vision and pattern recognition*, pages 695–704, 2018. 2, 3
 - [122] He Zhang and Vishal M Patel. Density-aware single image de-raining using a multi-stream dense network. In *CVPR*, 2018. 5
 - [123] Jinghao Zhang, Jie Huang, Mingde Yao, Zizheng Yang, Hu Yu, Man Zhou, and Feng Zhao. Ingredient-oriented multi-degradation learning for image restoration. In *Proceedings of the IEEE/CVF Conference on Computer Vision and Pattern Recognition*, pages 5825–5835, 2023. 3, 5
 - [124] Kai Zhang, Jingyun Liang, Luc Van Gool, and Radu Timofte. Designing a practical degradation model for deep blind image super-resolution. In *arxiv*, 2021. 1, 3, 6, 8
 - [125] Kai Zhang, Wangmeng Zuo, Yunjin Chen, Deyu Meng, and Lei Zhang. Beyond a gaussian denoiser: Residual learning of deep cnn for image denoising. *IEEE transactions on image processing*, 26(7):3142–3155, 2017. 2
 - [126] Kai Zhang, Wangmeng Zuo, and Lei Zhang. Ffdnet: Toward a fast and flexible solution for cnn-based image denoising. *IEEE Transactions on Image Processing*, 27(9):4608–4622, 2018. 2
 - [127] Kai Zhang, Wangmeng Zuo, and Lei Zhang. Learning a single convolutional super-resolution network for multiple degradations. In *Proceedings of the IEEE Conference on Computer Vision and Pattern Recognition*, pages 3262–3271, 2018. 8, 19
 - [128] Ruofan Zhang, Jinjin Gu, Haoyu Chen, Chao Dong, Yulun Zhang, and Wenming Yang. Crafting training degradation distribution for the accuracy-generalization trade-off. In *international conference on machine learning*. PMLR, 2023. 2
 - [129] Wenlong Zhang, Xiaohui Li, Xiangyu Chen, Xiaoyun Zhang, Yu Qiao, Xiao-Ming Wu, and Chao Dong. Seal: A framework for systematic evaluation of real-world super-resolution. In *The Twelfth International Conference on Learning Representations*, 2023. 7
 - [130] Wenlong Zhang, Xiaohui Li, Guangyuan Shi, Xiangyu Chen, Yu Qiao, Xiaoyun Zhang, Xiao-Ming Wu, and Chao Dong. Real-world image super-resolution as multi-task learning. *Advances in Neural Information Processing Systems*, 36, 2024. 11
 - [131] Hengyuan Zhao, Xiangtao Kong, Jingwen He, Yu Qiao, and Chao Dong. Efficient image super-resolution using pixel attention, 2020. 2

Appendix

In this appendix, we show the details of testing and training data including basic single tasks, mixed tasks selecting methods and the combination parameters & demo of the selected tasks. After that, we display more detailed results of the synthesized test set.

A. Details of Testing Data

A.1. Degradations

We select 10 existing well-defined tasks as basic single tasks in the main paper. They are `resize`, `blur`, `noise`, `compression`, `ringing`, `alg.artifact`, `damage`, `rain`, `haze` and `snow`. We show a demo of these single degradations in Figure C.1 (1 - 10), and put the degradation formulations and details as follow:

Resize.

$$I_{LQ} = \text{Upsample}(\text{Downsample}(I_{GT})), \quad (7)$$

where $\text{Downsample}()$ is a common operation to generate low-resolution images in super-resolution tasks [31], contains nearest-neighbor interpolation, bilinear interpolation, bicubic interpolation, and so on. In this work, to combine other degradations, we use $\text{Upsample}()$ to recover the low-resolution images to the original scale. We use the X4 scale bicubic as the $\text{Downsample}()$ and $\text{Upsample}()$ for the representative and random tasks.

Blur.

$$I_{LQ} = I_{GT} \otimes k, \quad (8)$$

where k is blur kernel. The isotropic and anisotropic Gaussian filters are common choices [127]. We use the isotropic Gaussian kernel with a kernel size of 15, $\sigma = 2$ for the representative task. For random blurring tasks, we sample the kernel size uniformly from 7 to 23, and sample σ uniformly from 0.2 to 3.

Noise.

$$I_{LQ} = I_{GT} + \epsilon, \quad (9)$$

where the ϵ can be synthesized by Gaussian noise, Poisson noise [1], etc. We use the Gaussian noise with a standard deviation of 20 for the representative task and sample standard deviation from 1 to 30 uniformly for random noise tasks.

Compression Artifacts.

$$I_{LQ} = \text{Compress}(I_{GT}). \quad (10)$$

Lossy compression post-processing, e.g., JPEG and JPEG2000, will bring block artifacts. We use the JPEG with a compression quality of 50 for the representative task and sample compression quality from 30 to 95 uniformly for random tasks.

Ring.

$$I_{LQ} = I_{GT} \otimes k, \quad (11)$$

where k is *sinc* filter kernel. It is an idealized filter that cuts off high frequencies, to synthesize ringing [106]. We use the *sinc* filter kernel with a kernel size of 15, and $\omega = 1.2$ for the representative task. We uniformly sample the kernel size from 7 to 23, and ω from $\pi/3$ to π for random tasks.

Restoration Algorithm Artifacts.

$$I_{LQ} = \text{Algorithm}(I_{GT}). \quad (12)$$

Many images from the Internet or smartphone cameras always have been processed by some simple restoration algorithm e.g. Richardson-Lucy algorithm [88, 73]. These algorithms make images look better but also bring grain and smearing-effect artifacts. We regard these artifacts as a type of degradations. We use the Richardson-Lucy algorithm as the $\text{Algorithm}()$ for the representative and random tasks.

Damage.

$$I_{LQ} = \text{Damage}(I_{GT}). \quad (13)$$

The goals of inpainting are various, from the restoration of damaged images to the removal/replacement of selected objects [5]. In GIR, we only focus on low-level vision damages such as scratches and lines. We use the white or black lines with the number 10 and thickness of 7 for representative tasks and the number 5 to 10, and thickness of 5 to 10 for random tasks.

Rain.

$$I_{LQ} = I_{LQ} + \text{rain}(\text{streak\&drop}), \quad (14)$$

where the *rain* is usually generated by the appearance and imaging process of rain (most from photoshop) [114, 33]. There are works to collect real rain data or generate the rain streak or raindrop by GAN [102]. We use the PhotoShop rain streaks synthesis method¹ with strength = 75 for representative tasks and strength = 50 to 100 for random tasks.

Haze.

$$I_{LQ} = I_{GT}t(I_{GT}) + A(1 - t(I_{GT})), \quad (15)$$

there are two critical parameters: A denotes the global atmospheric light, and $t(I_{GT})$ is the transmission matrix defined as:

$$t(I_{GT}) = e^{-\beta d(I_{GT})}, \quad (16)$$

where β is the scattering coefficient of the atmosphere, and $d(I_{GT})$ is the distance between the object and the camera. Nowadays, to obtain enough haze and haze-free pairs, researchers usually synthesize haze images by the above formulations [53]. They first estimate the depth map and then

¹This method is from <https://www.photoshopsentials.com/photo-effects/photoshop-weather-effects-rain/>

sample the value of β and A to generate haze images with different degrees. We use the method of [53] with $A = 0.9$, $\beta = 1.8$ for representative tasks and $A = 0.8$ to 1, $\beta = 0.5$ to 2.5 for random tasks.

Snow. The degradation model of snow is under development. We select an acceptable model [17]:

$$I_{LQ} = I_s t(I_{GT}) + A(1 - t(I_{GT})), \quad (17)$$

where A denotes the global atmospheric light, and $t(I_{GT})$ is the transmission matrix to construct the veiling effect of snow. These two parameters are the same as that in haze generation (see Eq. 15). I_s is the snowy images without the veiling effect, which can be formulated as

$$I_s = I_{GT}(1 - ZR) + CZR, \quad (18)$$

where R is a binary mask which presents the snow location information, C and Z are the chromatic aberration map for snow images and the snow mask, respectively. We use the method of [53] with $A = 0.9$, $\beta = 0.75$ for representative tasks and $A = 0.8$ to 0.95, $\beta = 0.5$ to 1 for random tasks, the snow makes are following [17].

A.2. Selecting Method of Representative Tasks

In the main paper, we select 50 representative tasks including single tasks. The ten single tasks are described in Section A.1. For other tasks with the degradation order numbers k are 2 to 5, we first generate lots of possible mixture tasks using random sequence and fixed strengths (See Section A.1). Then we execute clustering in each order following the method of [79, 100]. Specifically, we use the histogram similarity to construct the similarity matrix by all image samples. After that, the similarity matrix is used as the input of spectral clustering, which can generate separable clusters in the GIR degradation space. Finally, we utilize the degradation parameters of the cluster center as the representative tasks, which will be used to generate the test datasets for each order. In that way, we obtain the test datasets of 50 representative tasks.

A.3. Representative Tasks and Random Tasks

As described in Section A.2, we select representative tasks of degradations with moderate strengths. After that, we also generate 50 mixed tasks of degradations with random orders and strengths. We show the degradation details and AR/ER performance on Table C.1, and the demo images on Figure C.1. Note that, the detailed degradation orders and strengths of 50 random tasks (id 51 - 100) will not be released. Because these tasks are cross-validation set, training a special MIR 100 that only concentrates on the 100 tasks will become possible once they are public. It will hack this evaluation system, which is contrary to our original purpose.

B. Details of Training Data

We sample the clean ground truth images from DIV2K [3] and Flickr2K [97] datasets, including 3,450 images in total. We first estimate the depth of these images using the model of [61]. After that, we add the rain, haze and snow separately using the range of random degradation strengths in Section A.1. Only the haze and snow need the depth information. Finally, we obtain in total 13,800 images. The remaining degradations are applied to image patches on the fly with the range of random degradation strengths in Section A.1.

C. Details of Experiments

C.1. Details of Model Performance

We show the detailed results (See Table C.2) of the paragraph “Model Generality” in the main paper. These models are far from the ideal GIR model. Most models cannot maintain acceptable performance on most tasks (See the blue text).

C.2. Details of Exploration

Details of GIR vs MIR We show the detailed results (See Table C.3) of the paragraph “GIR vs MIR” in the main paper. It shows that although the MIR models can achieve acceptable even some excellence results on their training tasks, they can hardly generalize to other similar tasks.

Details of Training Data Scale Effect We show the detailed results (See Table C.4) of the paragraph “Training Data Scale Effect” in the main paper. It proves that the core bottleneck of GIR is not dataset scale. Surprisingly, adding ImageNet [29] images into the training set decreases the GIR performance. This confirms our conclusion that GIR needs high-quality images for training and testing, while the image quality of ImageNet is not desirable, containing noise and compression. Therefore, high-quality training data is still in demand for GIR.

Details of Training Strategy Effect We show the detailed results of the paragraph “Training Strategy Effect” in the main paper. Table C.5 is the effect of training patch size and Table C.6 is the effect of training batch size. we can see that all three metrics are improving with the increasing batch and patch size. But the marginal effect of this improvement is diminishing. We also find that models with large batch and patch sizes may achieve the excellence line in some degradations. All these degradations included snow or rain, illustrating that batch and patch sizes may have a greater impact on such degradations.

Task ID	Degradations	AR Model	ER Model
1	resize	25.33	26.10
2	Blur	30.74	32.41
3	Noise	32.32	33.61
4	compression	32.79	33.81
5	damage	31.93	35.81
6	ringing	29.91	35.03
7	alg.artifact	32.34	38.64
8	rain	25.82	37.87
9	haze	20.85	27.78
10	snow	21.49	27.77
11	rain + ringing	23.78	30.43
12	ringing + ringing	29.84	31.36
13	Noise + resize	24.30	25.05
14	compression + alg.artifact	30.03	33.04
15	haze + Noise	19.41	22.98
16	compression + damage	29.07	31.49
17	damage + alg.artifact	27.48	33.07
18	snow + compression	20.78	23.84
19	Noise + Blur	29.20	30.47
20	Noise + ringing	28.59	31.78
21	compression + damage + resize	23.23	25.18
22	alg.artifact + alg.artifact + damage	27.82	32.01
23	alg.artifact + Noise + alg.artifact	27.17	28.17
24	snow + compression + ringing	20.24	23.24
25	haze + resize + resize	18.86	21.82
26	rain + resize + resize	22.11	24.65
27	Noise + damage + damage	27.29	29.92
28	alg.artifact + ringing + Blur	28.14	29.63
29	snow + Blur + Noise	19.28	21.46
30	Noise + compression + resize	24.51	25.22
31	resize + ringing + damage + resize	23.48	25.23
32	haze + resize + resize + resize	18.70	21.79
33	Noise + damage + resize + ringing	22.49	24.32
34	rain + resize + resize + resize	22.37	24.73
35	snow + ringing + alg.artifact + ringing	19.94	23.25
36	Blur + ringing + Noise + damage	25.18	26.43
37	haze + resize + Blur + Noise	18.01	20.34
38	snow + Noise + Noise + Noise	19.96	22.68
39	Blur + Blur + Blur + Blur	25.95	27.39
40	Blur + ringing + ringing + alg.artifact	27.92	29.36
41	alg.artifact + resize + Blur + compression + damage	24.98	26.40
42	Noise + resize + damage + alg.artifact + resize	23.07	24.47
43	snow + ringing + damage + resize + resize	18.88	21.67
44	haze + Blur + alg.artifact + Noise + ringing	17.99	20.16
45	resize + resize + resize + resize + resize	25.33	26.06
46	rain + ringing + ringing + Noise + compression	22.35	25.17
47	snow + ringing + Blur + Noise + ringing	19.09	21.25
48	compression + Noise + Noise + ringing + Noise	26.86	27.90
49	Blur + resize + compression + ringing + Blur	26.09	26.92
50	haze + compression + damage + compression + Noise	18.22	21.62

Task ID	Degradations	AR Model	ER Model
51	-	25.34	26.10
52	-	32.12	33.76
53	-	31.00	32.29
54	-	31.65	32.65
55	-	32.27	36.11
56	-	32.49	37.47
57	-	32.34	38.64
58	-	24.89	35.31
59	-	20.71	27.97
60	-	21.22	27.38
61	-	25.15	25.79
62	-	30.11	33.10
63	-	30.59	33.31
64	-	31.52	32.53
65	-	32.73	36.10
66	-	31.05	36.74
67	-	27.44	28.48
68	-	22.52	28.33
69	-	24.86	28.93
70	-	21.72	27.18
71	-	25.33	26.06
72	-	26.38	27.36
73	-	30.31	32.49
74	-	27.74	30.02
75	-	24.52	26.91
76	-	31.87	33.07
77	-	27.02	28.94
78	-	22.44	28.72
79	-	17.53	21.53
80	-	20.93	24.81
81	-	24.62	25.42
82	-	26.23	27.12
83	-	28.64	30.40
84	-	28.56	29.53
85	-	25.75	28.85
86	-	26.68	27.49
87	-	25.77	26.60
88	-	23.81	30.54
89	-	22.82	24.61
90	-	18.89	20.87
91	-	24.97	25.62
92	-	25.52	26.31
93	-	24.96	25.68
94	-	26.40	27.31
95	-	25.36	30.56
96	-	28.15	29.71
97	-	26.34	27.02
98	-	23.39	27.58
99	-	17.41	21.61
100	-	19.84	21.92

Table C.1: Degradation details of the basic single tasks (1 - 10), representative tasks (1 - 50) and random tasks (51 - 100). We also show the PSNR (dB) of corresponding AR and ER models.

Task ID	AR Model	ER Model	DRL	RRDB	SwinIR	Uformer	Restormer	HAT
1	25.33	26.10	24.76	24.98	24.21	24.66	23.12	24.58
2	30.74	32.41	28.02	28.56	27.09	27.45	30.31	27.74
3	32.32	33.61	29.56	31.38	30.13	30.28	32.13	30.58
4	32.79	33.81	31.22	31.44	30.53	30.35	32.37	31.26
5	31.93	35.81	31.95	31.92	30.85	30.20	34.10	32.13
6	29.91	35.03	27.89	27.92	27.33	27.70	29.13	27.88
7	32.34	38.64	31.43	32.31	28.64	28.58	32.94	29.50
8	25.82	37.87	30.79	32.27	28.09	28.02	32.11	28.97
9	20.85	27.78	23.62	24.93	22.70	23.10	22.37	24.17
10	21.49	27.77	25.03	26.98	24.62	25.05	24.66	25.58
11	23.78	30.43	24.57	25.48	24.11	24.90	26.14	24.71
12	29.84	31.36	26.80	26.73	26.39	26.82	27.68	26.83
13	24.30	25.05	22.13	24.20	23.48	23.98	22.68	23.71
14	30.03	33.04	29.81	30.07	28.07	28.10	30.64	28.57
15	19.41	22.98	15.86	19.46	18.13	19.22	19.21	19.63
16	29.07	31.49	29.42	29.54	28.46	28.16	30.26	29.14
17	27.48	33.07	28.44	29.29	26.55	26.65	29.58	27.23
18	20.78	23.84	20.84	23.23	21.48	22.66	22.33	22.39
19	29.20	30.47	27.66	28.17	26.72	27.19	28.87	27.30
20	28.59	31.78	26.43	27.22	26.53	27.18	28.16	27.02
21	23.23	25.18	23.98	24.30	23.52	23.77	22.66	23.78
22	27.82	32.01	26.51	27.56	25.70	25.83	28.64	26.22
23	27.17	28.17	25.84	26.48	25.80	26.30	27.10	26.10
24	20.24	23.24	19.30	21.34	20.17	21.78	21.08	21.15
25	18.86	21.82	18.24	19.63	18.26	19.25	17.88	19.40
26	22.11	24.65	22.99	23.53	22.32	23.03	22.35	22.90
27	27.29	29.92	27.39	28.11	26.82	26.63	28.57	27.35
28	28.14	29.63	26.03	26.89	25.93	26.25	27.91	26.33
29	19.28	21.46	17.92	20.55	19.17	20.70	19.96	20.16
30	24.51	25.22	24.12	24.26	23.72	24.09	22.91	24.04
31	23.48	25.23	23.89	24.26	23.56	23.84	22.79	23.88
32	18.70	21.79	18.22	19.62	18.24	19.25	17.88	19.38
33	22.49	24.32	21.27	22.82	21.73	21.88	22.31	22.81
34	22.37	24.73	23.12	23.64	22.36	23.12	22.46	23.01
35	19.94	23.25	20.99	22.31	21.33	22.08	21.30	22.03
36	25.18	26.43	24.43	24.88	23.98	24.42	25.40	24.42
37	18.01	20.34	13.54	16.74	15.94	16.83	16.92	16.90
38	19.96	22.68	18.13	21.88	19.63	21.53	21.23	20.62
39	25.95	27.39	23.80	24.95	23.57	24.40	26.07	24.02
40	27.92	29.36	25.16	25.99	25.33	25.48	26.47	25.65
41	24.98	26.40	24.67	24.99	24.05	24.26	24.89	24.53
42	23.07	24.47	22.65	23.52	22.86	23.35	21.99	23.17
43	18.88	21.67	19.42	21.27	20.14	20.99	19.64	20.94
44	17.99	20.16	11.82	15.97	14.91	16.11	16.85	15.67
45	25.33	26.06	24.69	24.96	24.15	24.60	23.06	24.52
46	22.35	25.17	22.44	23.20	22.21	22.75	24.02	22.80
47	19.09	21.25	16.50	19.83	18.70	19.96	19.44	19.93
48	26.86	27.90	25.27	26.04	25.46	25.96	26.61	25.77
49	26.09	26.92	24.75	24.74	24.70	25.12	24.13	25.03
50	18.22	21.62	14.98	17.59	16.29	17.33	17.55	17.36

Task ID	AR Model	ER Model	DRL	RRDB	SwinIR	Uformer	Restormer	HAT
51	25.34	26.10	24.76	24.98	24.21	24.66	23.12	24.58
52	32.12	33.76	28.93	29.41	27.54	27.92	31.31	28.43
53	31.00	32.29	27.91	30.31	29.13	29.39	30.93	29.58
54	31.65	32.65	30.37	30.48	29.59	29.31	31.32	30.26
55	32.27	36.11	31.94	32.11	31.05	30.45	34.51	32.43
56	32.49	37.47	30.10	30.09	29.61	29.61	31.61	30.25
57	32.34	38.64	31.43	32.31	28.64	28.58	32.94	29.50
58	24.89	35.31	28.60	30.28	26.70	26.74	30.04	27.54
59	20.71	27.97	22.53	22.03	21.03	21.32	21.02	22.08
60	21.22	27.38	24.35	26.33	23.91	24.42	23.96	24.90
61	25.15	25.79	24.65	24.87	24.02	24.54	23.06	24.39
62	30.11	33.10	27.70	28.07	26.95	27.43	29.57	27.48
63	30.59	33.31	30.19	31.03	29.79	29.25	31.88	30.41
64	31.52	32.53	30.15	30.56	29.72	29.54	31.16	30.21
65	32.73	36.10	32.03	33.21	31.88	31.08	34.29	32.62
66	31.05	36.74	29.64	29.54	28.78	28.47	30.97	29.50
67	27.44	28.48	25.55	26.81	25.68	26.45	27.54	26.00
68	22.52	28.33	24.36	25.18	22.76	23.66	25.68	23.55
69	24.86	28.93	25.85	26.89	25.42	25.11	26.39	26.64
70	21.72	27.18	24.05	25.06	23.65	23.99	24.51	24.46
71	25.33	26.06	24.70	24.88	24.04	24.51	22.98	24.35
72	26.38	27.36	25.26	25.76	24.82	25.25	26.50	25.31
73	30.31	32.49	27.04	28.07	27.41	27.67	29.04	27.83
74	27.74	30.02	27.26	28.48	27.27	27.19	28.89	27.72
75	24.52	26.91	24.52	24.90	24.39	24.63	23.37	24.62
76	31.87	33.07	29.04	29.68	28.91	28.68	30.73	29.24
77	27.02	28.94	26.03	27.17	25.80	26.49	27.91	26.13
78	22.44	28.72	24.76	26.43	24.14	24.29	26.58	24.90
79	17.53	21.53	15.51	17.21	15.22	16.07	17.56	16.35
80	20.93	24.81	22.30	23.71	22.30	22.91	22.96	22.84
81	24.62	25.42	22.75	24.50	23.52	24.13	23.05	23.83
82	26.23	27.12	24.79	25.53	24.37	24.88	26.27	24.89
83	28.64	30.40	26.24	28.70	27.59	27.69	29.17	28.02
84	28.56	29.53	26.49	27.38	26.56	27.10	28.28	26.85
85	25.75	28.85	24.85	26.19	24.89	25.22	26.89	25.22
86	26.68	27.49	25.61	25.64	24.83	25.25	23.38	25.29
87	25.77	26.60	24.43	25.27	24.61	25.16	23.92	24.89
88	23.81	30.54	25.31	26.37	24.65	25.09	27.05	25.45
89	22.82	24.61	20.90	21.23	20.88	21.63	21.79	21.55
90	18.89	20.87	17.61	20.04	18.88	20.18	18.88	19.74
91	24.97	25.62	24.46	24.72	23.96	24.29	22.96	24.05
92	25.52	26.31	24.44	24.86	24.07	24.10	24.73	24.54
93	24.96	25.68	23.76	24.28	23.84	24.18	24.90	24.26
94	26.40	27.31	23.83	25.69	24.58	25.80	26.31	25.45
95	25.36	30.56	27.02	27.60	26.44	26.55	28.36	27.34
96	28.15	29.71	27.17	27.77	26.93	27.09	28.31	27.39
97	26.34	27.02	25.71	25.66	25.15	25.39	23.38	25.38
98	23.39	27.58	23.72	24.49	23.39	24.14	25.53	23.81
99	17.41	21.61	13.16	16.19	15.46	16.55	16.66	16.29
100	19.84	21.92	19.43	21.10	20.15	21.17	19.68	21.19

Table C.2: Detailed PSNR (dB) of different GIR baseline models (paragraph “Model Generality” in the main paper). The results that surpass the corresponding AR/ER model are marked with **Blue** and **Red**. No model can surpass the corresponding ER models.

Task ID	AR Model	ER Model	MIR 10	MIR 50	GIR
1	25.33	26.10	25.11	25.72	24.98
2	30.74	32.41	30.40	31.68	28.56
3	32.32	33.61	30.16	33.05	31.38
4	32.79	33.81	31.88	33.14	31.44
5	31.93	35.81	32.78	34.01	31.92
6	29.91	35.03	31.74	34.12	27.92
7	32.34	38.64	34.25	37.54	32.31
8	25.82	37.87	30.86	34.89	32.27
9	20.85	27.78	26.76	30.30	24.93
10	21.49	27.77	27.31	30.16	26.98
11	23.78	30.43	27.46	18.75	25.48
12	29.84	31.36	29.56	28.16	26.73
13	24.30	25.05	24.57	23.12	24.20
14	30.03	33.04	31.33	31.06	30.07
15	19.41	22.98	22.83	11.10	19.46
16	29.07	31.49	29.94	29.32	29.54
17	27.48	33.07	29.70	17.82	29.29
18	20.78	23.84	23.69	14.73	23.23
19	29.20	30.47	29.57	28.23	28.17
20	28.59	31.78	28.80	27.87	27.22
21	23.23	25.18	24.48	17.05	24.30
22	27.82	32.01	29.14	25.68	27.56
23	27.17	28.17	27.60	24.25	26.48
24	20.24	23.24	23.59	14.69	21.34
25	18.86	21.82	21.87	11.00	19.63
26	22.11	24.65	23.77	18.40	23.53
27	27.29	29.92	27.96	20.88	28.11
28	28.14	29.63	28.23	25.68	26.89
29	19.28	21.46	21.56	14.20	20.55
30	24.51	25.22	24.77	24.32	24.26
31	23.48	25.23	24.35	17.08	24.26
32	18.70	21.79	21.94	11.01	19.62
33	22.49	24.32	23.80	16.94	22.82
34	22.37	24.73	23.91	18.92	23.64
35	19.94	23.25	23.30	14.45	22.31
36	25.18	26.43	25.26	20.51	24.88
37	18.01	20.34	20.09	10.83	16.74
38	19.96	22.68	23.15	14.29	21.88
39	25.95	27.39	26.23	22.88	24.95
40	27.92	29.36	28.04	24.90	25.99
41	24.98	26.40	25.61	23.88	24.99
42	23.07	24.47	23.84	17.25	23.52
43	18.88	21.67	21.90	12.68	21.27
44	17.99	20.16	19.70	10.75	15.97
45	25.33	26.06	24.96	25.65	24.96
46	22.35	25.17	23.95	18.62	23.20
47	19.09	21.25	21.55	14.02	19.83
48	26.86	27.90	27.32	25.70	26.04
49	26.09	26.92	25.94	24.06	24.74
50	18.22	21.62	21.55	10.31	17.59

Task ID	AR Model	ER Model	MIR 10	MIR 50	GIR
51	25.34	26.10	25.11	25.72	24.98
52	32.12	33.76	25.48	23.95	29.41
53	31.00	32.29	29.26	30.49	30.31
54	31.65	32.65	30.93	31.89	30.48
55	32.27	36.11	32.89	34.32	32.11
56	32.49	37.47	24.72	17.35	30.09
57	32.34	38.64	34.25	37.54	32.31
58	24.89	35.31	28.07	31.79	30.28
59	20.71	27.97	21.93	21.50	22.03
60	21.22	27.38	26.41	29.90	26.33
61	25.15	25.79	24.35	24.64	24.87
62	30.11	33.10	27.75	28.03	28.07
63	30.59	33.31	30.44	30.39	31.03
64	31.52	32.53	30.41	30.52	30.56
65	32.73	36.10	31.38	27.28	33.21
66	31.05	36.74	26.94	19.66	29.54
67	27.44	28.48	24.47	25.90	26.81
68	22.52	28.33	16.82	15.14	25.18
69	24.86	28.93	20.68	20.76	26.89
70	21.72	27.18	23.63	16.29	25.06
71	25.33	26.06	24.84	25.11	24.88
72	26.38	27.36	26.35	24.35	25.76
73	30.31	32.49	24.70	19.91	28.07
74	27.74	30.02	25.10	18.91	28.48
75	24.52	26.91	18.48	18.61	24.90
76	31.87	33.07	28.72	29.71	29.68
77	27.02	28.94	24.07	20.50	27.17
78	22.44	28.72	16.81	14.88	26.43
79	17.53	21.53	9.41	9.25	17.21
80	20.93	24.81	16.84	15.87	23.71
81	24.62	25.42	22.99	23.16	24.50
82	26.23	27.12	26.06	23.85	25.53
83	28.64	30.40	27.28	18.90	28.70
84	28.56	29.53	25.88	27.33	27.38
85	25.75	28.85	17.92	17.44	26.19
86	26.68	27.49	25.11	24.44	25.64
87	25.77	26.60	24.00	25.13	25.27
88	23.81	30.54	23.66	15.70	26.37
89	22.82	24.61	18.03	18.42	21.23
90	18.89	20.87	20.63	13.99	20.04
91	24.97	25.62	23.21	19.34	24.72
92	25.52	26.31	25.24	23.94	24.86
93	24.96	25.68	24.24	22.65	24.28
94	26.40	27.31	25.10	18.81	25.69
95	25.36	30.56	17.70	17.56	27.60
96	28.15	29.71	27.37	20.32	27.77
97	26.34	27.02	25.36	25.33	25.66
98	23.39	27.58	18.67	17.69	24.49
99	17.41	21.61	10.00	9.16	16.19
100	19.84	21.92	19.71	15.20	21.10

Table C.3: Detailed PSNR (dB) of MIR and GIR models (paragraph “GIR vs MIR” in the main paper). The results that surpass the corresponding AR/ER model are marked with **Blue** and **Red**.

Task ID	AR Model	ER Model	Quarter of DF2K	Half of DF2K	All of DF2K	ImageNet + DF2K
1	25.33	26.10	24.99	24.85	24.98	23.04
2	30.74	32.41	28.53	28.30	28.56	28.40
3	32.32	33.61	31.39	31.22	31.38	31.30
4	32.79	33.81	31.28	31.20	31.44	31.03
5	31.93	35.81	31.94	31.48	31.92	30.55
6	29.91	35.03	28.07	27.57	27.92	28.01
7	32.34	38.64	32.40	32.25	32.31	33.45
8	25.82	37.87	32.23	31.90	32.27	32.47
9	20.85	27.78	24.77	24.60	24.93	25.30
10	21.49	27.77	27.04	26.78	26.98	27.08
11	23.78	30.43	25.69	25.46	25.48	25.55
12	29.84	31.36	26.96	26.60	26.73	26.85
13	24.30	25.05	24.17	24.17	24.20	22.54
14	30.03	33.04	30.06	29.98	30.07	30.28
15	19.41	22.98	19.65	19.13	19.46	20.60
16	29.07	31.49	29.55	29.40	29.54	29.39
17	27.48	33.07	29.22	29.26	29.29	30.31
18	20.78	23.84	23.35	22.94	23.23	23.05
19	29.20	30.47	28.01	27.98	28.17	28.05
20	28.59	31.78	27.28	27.02	27.22	27.11
21	23.23	25.18	24.25	24.13	24.30	22.71
22	27.82	32.01	27.74	27.53	27.56	27.98
23	27.17	28.17	26.47	26.35	26.48	26.45
24	20.24	23.24	21.51	21.16	21.34	21.22
25	18.86	21.82	19.40	19.20	19.63	19.37
26	22.11	24.65	23.52	23.51	23.53	22.38
27	27.29	29.92	28.16	28.05	28.11	28.26
28	28.14	29.63	26.87	26.75	26.89	26.88
29	19.28	21.46	20.60	20.37	20.55	20.53
30	24.51	25.22	24.23	24.27	24.26	22.80
31	23.48	25.23	24.28	24.16	24.26	22.78
32	18.70	21.79	19.37	19.19	19.62	19.29
33	22.49	24.32	23.14	22.79	22.82	22.29
34	22.37	24.73	23.61	23.59	23.64	22.43
35	19.94	23.25	22.46	22.36	22.31	22.57
36	25.18	26.43	24.92	24.84	24.88	24.85
37	18.01	20.34	17.07	16.50	16.74	17.85
38	19.96	22.68	22.04	21.58	21.88	21.83
39	25.95	27.39	25.04	24.93	24.95	24.65
40	27.92	29.36	26.07	25.91	25.99	25.95
41	24.98	26.40	25.02	24.94	24.99	24.44
42	23.07	24.47	23.46	23.42	23.52	22.23
43	18.88	21.67	21.35	21.09	21.27	20.70
44	17.99	20.16	15.95	15.63	15.97	16.82
45	25.33	26.06	24.93	24.82	24.96	22.98
46	22.35	25.17	23.23	23.14	23.20	23.12
47	19.09	21.25	19.77	19.54	19.83	19.94
48	26.86	27.90	26.04	25.91	26.04	25.97
49	26.09	26.92	24.75	24.71	24.74	23.60
50	18.22	21.62	17.93	17.37	17.59	18.83

Task ID	AR Model	ER Model	Quarter of DF2K	Half of DF2K	All of DF2K	ImageNet + DF2K
51	25.34	26.10	24.99	24.85	24.98	23.04
52	32.12	33.76	29.37	29.06	29.41	29.24
53	31.00	32.29	30.33	30.16	30.31	30.27
54	31.65	32.65	30.36	30.11	30.48	30.04
55	32.27	36.11	32.12	31.61	32.11	30.72
56	32.49	37.47	30.27	29.86	30.09	29.68
57	32.34	38.64	32.40	32.25	32.31	33.45
58	24.89	35.31	30.21	29.95	30.28	30.29
59	20.71	27.97	21.88	21.78	22.03	22.75
60	21.22	27.38	26.31	26.03	26.33	26.28
61	25.15	25.79	24.84	24.78	24.87	23.07
62	30.11	33.10	28.24	28.07	28.07	28.37
63	30.59	33.31	31.03	30.93	31.03	30.96
64	31.52	32.53	30.52	30.40	30.56	30.32
65	32.73	36.10	33.15	33.04	33.21	33.02
66	31.05	36.74	29.72	29.36	29.54	29.18
67	27.44	28.48	26.79	26.70	26.81	26.65
68	22.52	28.33	25.00	24.94	25.18	25.34
69	24.86	28.93	27.07	26.69	26.89	28.05
70	21.72	27.18	25.15	25.06	25.06	25.65
71	25.33	26.06	24.90	24.78	24.88	22.96
72	26.38	27.36	25.85	25.74	25.76	25.40
73	30.31	32.49	27.95	27.81	28.07	27.77
74	27.74	30.02	28.49	28.34	28.48	28.39
75	24.52	26.91	24.74	24.70	24.90	23.21
76	31.87	33.07	29.63	29.57	29.68	29.32
77	27.02	28.94	27.09	27.08	27.17	27.02
78	22.44	28.72	26.39	26.24	26.43	26.46
79	17.53	21.53	17.17	16.89	17.21	17.77
80	20.93	24.81	23.90	23.77	23.71	24.11
81	24.62	25.42	24.45	24.39	24.50	22.85
82	26.23	27.12	25.57	25.51	25.53	25.28
83	28.64	30.40	28.70	28.56	28.70	28.69
84	28.56	29.53	27.37	27.30	27.38	27.28
85	25.75	28.85	26.24	26.16	26.19	26.42
86	26.68	27.49	25.67	25.56	25.64	23.24
87	25.77	26.60	25.26	25.18	25.27	23.53
88	23.81	30.54	26.34	26.26	26.37	26.30
89	22.82	24.61	21.07	21.01	21.23	22.12
90	18.89	20.87	20.05	19.83	20.04	19.77
91	24.97	25.62	24.75	24.67	24.72	23.50
92	25.52	26.31	24.90	24.83	24.86	24.40
93	24.96	25.68	24.28	24.30	24.28	24.21
94	26.40	27.31	25.43	25.54	25.69	25.53
95	25.36	30.56	27.59	27.43	27.60	27.94
96	28.15	29.71	27.78	27.66	27.77	27.69
97	26.34	27.02	25.65	25.49	25.66	23.34
98	23.39	27.58	24.35	24.13	24.49	24.17
99	17.41	21.61	16.89	16.06	16.19	16.88
100	19.84	21.92	21.07	20.90	21.10	20.38

Table C.4: Detailed PSNR (dB) of GIR-RRDB trained with different scale of data (paragraph “Training Data Scale Effect” in the main paper). The results that surpass the corresponding AR/ER model are marked with **Blue** and **Red**. No model can surpass the corresponding ER models.

Task ID	AR Model	ER Model	PS 64	PS 128	PS 192	PS 256
1	25.33	26.10	24.71	24.98	25.10	25.25
2	30.74	32.41	27.85	28.56	28.83	29.26
3	32.32	33.61	30.75	31.38	31.61	31.71
4	32.79	33.81	30.79	31.44	31.60	31.62
5	31.93	35.81	29.89	31.92	32.39	33.05
6	29.91	35.03	27.52	27.92	28.02	28.47
7	32.34	38.64	31.37	32.31	32.91	33.48
8	25.82	37.87	30.57	32.27	32.81	33.40
9	20.85	27.78	23.54	24.93	25.50	25.76
10	21.49	27.77	25.82	26.98	27.68	28.05
11	23.78	30.43	24.78	25.48	25.76	25.97
12	29.84	31.36	26.60	26.73	26.86	27.22
13	24.30	25.05	23.83	24.20	24.26	24.38
14	30.03	33.04	29.53	30.07	30.37	30.51
15	19.41	22.98	17.67	19.46	19.82	20.34
16	29.07	31.49	28.92	29.54	29.76	29.86
17	27.48	33.07	28.68	29.29	29.44	29.94
18	20.78	23.84	21.77	23.23	23.65	24.06
19	29.20	30.47	27.48	28.17	28.22	28.44
20	28.59	31.78	26.75	27.22	27.25	27.50
21	23.23	25.18	23.89	24.30	24.41	24.52
22	27.82	32.01	26.39	27.56	27.98	28.48
23	27.17	28.17	26.04	26.48	26.55	26.84
24	20.24	23.24	19.49	21.34	21.84	22.47
25	18.86	21.82	17.98	19.63	19.84	20.16
26	22.11	24.65	22.92	23.53	23.74	23.97
27	27.29	29.92	27.51	28.11	28.34	28.50
28	28.14	29.63	26.52	26.89	27.13	27.33
29	19.28	21.46	19.07	20.55	20.98	21.22
30	24.51	25.22	23.98	24.26	24.39	24.47
31	23.48	25.23	23.96	24.26	24.40	24.51
32	18.70	21.79	17.96	19.62	19.85	20.17
33	22.49	24.32	22.06	22.82	23.45	23.44
34	22.37	24.73	23.02	23.64	23.83	24.07
35	19.94	23.25	21.15	22.31	22.75	23.06
36	25.18	26.43	24.64	24.88	24.98	25.15
37	18.01	20.34	15.22	16.74	17.27	17.72
38	19.96	22.68	20.13	21.88	22.22	22.57
39	25.95	27.39	24.51	24.95	25.21	25.48
40	27.92	29.36	25.72	25.99	26.24	26.37
41	24.98	26.40	24.63	24.99	25.08	25.20
42	23.07	24.47	23.16	23.52	23.56	23.61
43	18.88	21.67	20.04	21.27	21.64	21.92
44	17.99	20.16	14.24	15.97	16.52	16.82
45	25.33	26.06	24.67	24.96	25.05	25.20
46	22.35	25.17	22.52	23.20	23.42	23.58
47	19.09	21.25	18.19	19.83	20.31	20.47
48	26.86	27.90	25.73	26.04	26.10	26.21
49	26.09	26.92	24.49	24.74	24.90	25.00
50	18.22	21.62	15.86	17.59	18.14	18.75

Task ID	AR Model	ER Model	PS 64	PS 128	PS 192	PS 256
51	25.34	26.10	24.71	24.98	25.10	25.25
52	32.12	33.76	28.55	29.41	29.72	30.16
53	31.00	32.29	29.69	30.31	30.49	30.60
54	31.65	32.65	29.86	30.48	30.58	30.60
55	32.27	36.11	30.08	32.11	32.56	33.25
56	32.49	37.47	29.59	30.09	30.55	30.81
57	32.34	38.64	31.37	32.31	32.91	33.48
58	24.89	35.31	28.73	30.28	30.67	31.22
59	20.71	27.97	20.94	22.03	22.70	22.90
60	21.22	27.38	25.17	26.33	26.88	27.24
61	25.15	25.79	24.65	24.87	24.92	25.03
62	30.11	33.10	27.68	28.07	28.37	28.82
63	30.59	33.31	30.18	31.03	31.28	31.52
64	31.52	32.53	29.99	30.56	30.67	30.69
65	32.73	36.10	32.12	33.21	33.52	33.78
66	31.05	36.74	28.97	29.54	30.03	30.30
67	27.44	28.48	26.34	26.81	26.90	27.11
68	22.52	28.33	24.13	25.18	25.43	25.94
69	24.86	28.93	25.43	26.89	27.62	27.91
70	21.72	27.18	23.85	25.06	25.87	26.24
71	25.33	26.06	24.61	24.88	24.98	25.13
72	26.38	27.36	25.38	25.76	25.84	25.96
73	30.31	32.49	27.57	28.07	28.04	28.24
74	27.74	30.02	27.88	28.48	28.62	28.73
75	24.52	26.91	24.34	24.90	25.17	25.52
76	31.87	33.07	29.13	29.68	29.83	30.06
77	27.02	28.94	26.67	27.17	27.30	27.46
78	22.44	28.72	25.38	26.43	26.74	27.09
79	17.53	21.53	15.17	17.21	17.69	18.23
80	20.93	24.81	22.52	23.71	24.44	24.72
81	24.62	25.42	24.12	24.50	24.52	24.70
82	26.23	27.12	25.13	25.53	25.67	25.78
83	28.64	30.40	28.13	28.70	28.81	28.92
84	28.56	29.53	26.89	27.38	27.53	27.67
85	25.75	28.85	25.57	26.19	26.45	26.65
86	26.68	27.49	25.35	25.64	25.75	25.86
87	25.77	26.60	24.92	25.27	25.36	25.54
88	23.81	30.54	25.45	26.37	26.74	26.98
89	22.82	24.61	19.99	21.23	21.51	21.85
90	18.89	20.87	18.63	20.04	20.34	20.56
91	24.97	25.62	24.21	24.72	24.78	24.92
92	25.52	26.31	24.48	24.86	24.99	25.10
93	24.96	25.68	24.06	24.28	24.47	24.53
94	26.40	27.31	25.01	25.69	25.68	25.86
95	25.36	30.56	26.82	27.60	27.98	28.06
96	28.15	29.71	27.34	27.77	27.85	28.03
97	26.34	27.02	25.02	25.66	25.84	25.92
98	23.39	27.58	23.63	24.49	24.74	25.05
99	17.41	21.61	14.39	16.19	16.92	17.71
100	19.84	21.92	19.85	21.10	21.65	21.86

Table C.5: Detailed PSNR (dB) of GIR-RRDB trained with different patch sizes (paragraph “Training Strategy Effect” in the main paper). The results that surpass the corresponding AR/ER model are marked with **Blue** and **Red**.

Task ID	AR Model	ER Model	BS4	BS8	BS16	BS32
1	25.33	26.10	24.81	24.98	25.10	25.33
2	30.74	32.41	28.11	28.56	28.93	29.54
3	32.32	33.61	31.04	31.38	31.54	31.92
4	32.79	33.81	30.98	31.44	31.49	31.89
5	31.93	35.81	30.75	31.92	32.61	33.57
6	29.91	35.03	27.55	27.92	28.20	28.54
7	32.34	38.64	31.49	32.31	33.16	34.22
8	25.82	37.87	30.87	32.27	33.25	34.08
9	20.85	27.78	23.74	24.93	25.51	26.25
10	21.49	27.77	25.92	26.98	27.86	28.55
11	23.78	30.43	25.21	25.48	25.85	26.05
12	29.84	31.36	26.69	26.73	26.94	27.21
13	24.30	25.05	24.01	24.20	24.32	24.38
14	30.03	33.04	29.56	30.07	30.31	30.83
15	19.41	22.98	18.66	19.46	20.06	20.25
16	29.07	31.49	29.16	29.54	29.73	30.05
17	27.48	33.07	28.50	29.29	29.84	30.50
18	20.78	23.84	22.26	23.23	23.83	24.26
19	29.20	30.47	27.77	28.17	28.32	28.55
20	28.59	31.78	26.96	27.22	27.38	27.56
21	23.23	25.18	24.05	24.30	24.37	24.58
22	27.82	32.01	26.83	27.56	28.10	28.86
23	27.17	28.17	26.24	26.48	26.61	26.85
24	20.24	23.24	20.12	21.34	22.16	22.51
25	18.86	21.82	18.74	19.63	20.09	20.91
26	22.11	24.65	23.29	23.53	23.78	24.02
27	27.29	29.92	27.79	28.11	28.36	28.56
28	28.14	29.63	26.57	26.89	27.09	27.54
29	19.28	21.46	19.77	20.55	20.95	21.22
30	24.51	25.22	24.07	24.26	24.44	24.62
31	23.48	25.23	24.10	24.26	24.40	24.58
32	18.70	21.79	18.73	19.62	20.10	20.89
33	22.49	24.32	22.43	22.82	23.33	23.60
34	22.37	24.73	23.39	23.64	23.88	24.13
35	19.94	23.25	21.69	22.31	22.79	23.13
36	25.18	26.43	24.76	24.88	25.02	25.16
37	18.01	20.34	15.92	16.74	17.30	17.62
38	19.96	22.68	20.82	21.88	22.44	22.85
39	25.95	27.39	24.81	24.95	25.33	25.62
40	27.92	29.36	25.80	25.99	26.13	26.54
41	24.98	26.40	24.75	24.99	25.16	25.26
42	23.07	24.47	23.31	23.52	23.49	23.58
43	18.88	21.67	20.59	21.27	21.69	22.09
44	17.99	20.16	14.72	15.97	15.89	16.33
45	25.33	26.06	24.75	24.96	25.04	25.29
46	22.35	25.17	22.89	23.20	23.33	23.63
47	19.09	21.25	18.97	19.83	19.89	20.28
48	26.86	27.90	25.82	26.04	26.10	26.21
49	26.09	26.92	24.58	24.74	24.87	25.16
50	18.22	21.62	16.75	17.59	18.39	18.54

Task ID	AR Model	ER Model	BS4	BS8	BS16	BS32
51	25.34	26.10	24.81	24.98	25.10	25.33
52	32.12	33.76	28.83	29.41	29.81	30.47
53	31.00	32.29	29.97	30.31	30.50	30.74
54	31.65	32.65	30.10	30.48	30.55	30.77
55	32.27	36.11	30.91	32.11	32.84	33.83
56	32.49	37.47	29.78	30.09	30.56	31.24
57	32.34	38.64	31.49	32.31	33.16	34.22
58	24.89	35.31	29.02	30.28	31.16	31.81
59	20.71	27.97	21.36	22.03	22.62	23.46
60	21.22	27.38	25.30	26.33	27.08	27.77
61	25.15	25.79	24.67	24.87	24.96	25.08
62	30.11	33.10	27.82	28.07	28.44	29.20
63	30.59	33.31	30.60	31.03	31.26	31.72
64	31.52	32.53	30.27	30.56	30.62	30.90
65	32.73	36.10	32.57	33.21	33.48	34.11
66	31.05	36.74	29.18	29.54	30.17	30.83
67	27.44	28.48	26.57	26.81	26.92	27.18
68	22.52	28.33	24.37	25.18	25.68	26.26
69	24.86	28.93	26.24	26.89	27.49	28.19
70	21.72	27.18	24.07	25.06	25.93	26.79
71	25.33	26.06	24.75	24.88	25.01	25.16
72	26.38	27.36	25.59	25.76	25.93	25.96
73	30.31	32.49	27.77	28.07	27.97	28.33
74	27.74	30.02	28.15	28.48	28.68	28.84
75	24.52	26.91	24.45	24.90	25.28	25.76
76	31.87	33.07	29.22	29.68	29.80	30.23
77	27.02	28.94	26.89	27.17	27.28	27.62
78	22.44	28.72	25.56	26.43	27.07	27.54
79	17.53	21.53	15.86	17.21	18.10	18.58
80	20.93	24.81	22.65	23.71	24.54	24.97
81	24.62	25.42	24.33	24.50	24.59	24.69
82	26.23	27.12	25.25	25.53	25.68	25.82
83	28.64	30.40	28.35	28.70	28.89	29.03
84	28.56	29.53	27.13	27.38	27.49	27.75
85	25.75	28.85	25.81	26.19	26.51	26.98
86	26.68	27.49	25.48	25.64	25.75	26.00
87	25.77	26.60	25.12	25.27	25.34	25.47
88	23.81	30.54	25.90	26.37	26.91	27.42
89	22.82	24.61	20.66	21.23	21.38	21.76
90	18.89	20.87	19.35	20.04	20.29	20.51
91	24.97	25.62	24.50	24.72	24.81	25.00
92	25.52	26.31	24.59	24.86	25.00	25.10
93	24.96	25.68	24.12	24.28	24.40	24.60
94	26.40	27.31	25.33	25.69	25.72	25.93
95	25.36	30.56	27.23	27.60	27.88	28.24
96	28.15	29.71	27.51	27.77	27.85	28.06
97	26.34	27.02	25.40	25.66	25.74	25.94
98	23.39	27.58	23.96	24.49	24.74	25.01
99	17.41	21.61	15.78	16.19	16.72	17.14
100	19.84	21.92	20.37	21.10	21.44	21.74

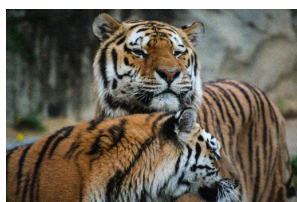
Table C.6: Detailed PSNR (dB) of GIR-RRDB trained with different batch sizes (paragraph “Training Strategy Effect” in the main paper). The results that surpass the corresponding AR/ER model are marked with **Blur** and **Red**.



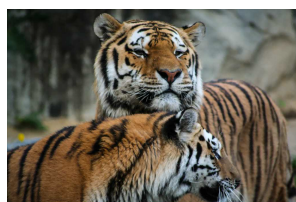
1



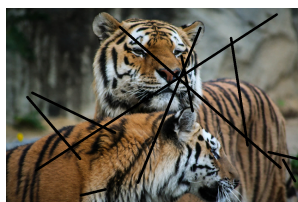
2



3



4



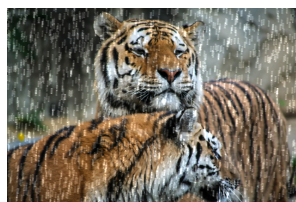
5



6



7



8



9



10



11



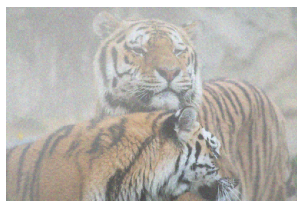
12



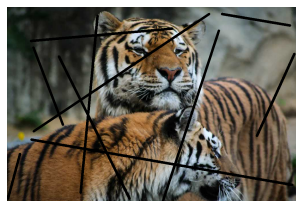
13



14



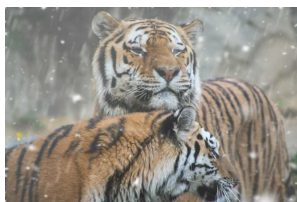
15



16



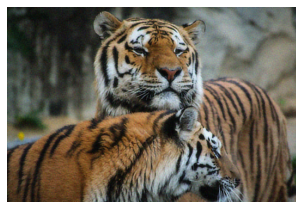
17



18



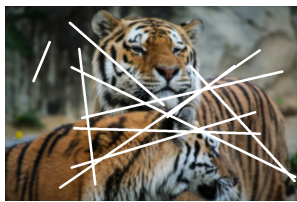
19



20



21



22



23



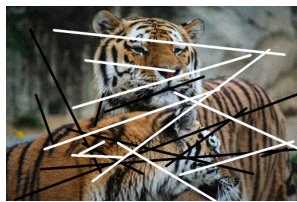
24



25



26



27



28



Figure C.1: The image demo of the basic single tasks (1 - 10), representative tasks (1 - 50). Zoom in for a better view.